Supporting Information (SI Appendix)

Predicting glycosaminoglycan-surface protein interactions: Implications for studying axonal growth

Adam R. Griffith,[a,b,1] Claude J. Rogers,[b,1] Gregory M. Miller,[b] Ravinder Abrol,[a,b] Linda C. Hsieh-Wilson,[b] and William A. Goddard III[a,b,*]

[a]Materials and Process Simulation Center,

California Institute of Technology, Pasadena, CA 91125

[b]Division of Chemistry and Chemical Engineering

California Institute of Technology, Pasadena, CA 91125,

[1] These two authors contributed equally

[*] To whom correspondence should be addressed; email: wagoddard3@gmail.com

Materials and Methods

System Preparation

Crystal structures & PTPσ. Protein residues within 5 Å of the GAG ligand, if present, were selected from the PDB. Hydrogen atoms were added with tleap (1) and CHARMM charges were assigned to each atom. The system was minimized using the DREIDING force field (2).

NgR. Five homology models for full-length NgR1, 2, and 3 were obtained using ROSETTA (3). Each model was conjugate gradient minimized (5000 steps) and then allowed to relax in the presence of water and counter ions with 5 ns of MD. MD was performed using NAMD in four steps, as described later in the MD section. Briefly, first, a water box bounding the protein was minimized with the protein kept fixed. Second, 0.5 ns of NPT MD were performed on the water box. Third, the entire systems were minimized. Finally, 5 ns of NPT MD were performed on the entire system. For each initial conformation, the conformation closest to the average structure from the 5 ns MD was minimized and the lowest energy conformation was selected for each isoform.

Ligand Preparation

For the four validation systems, the ligand found in the crystal structure was used. The CS-A, CS-D, and CS-E structures used for docking to the non-validation systems were based on a CS-A hexasaccharide crystal structure (4), while the heparin structures for docking to the non-validation systems are based on a heparin 18-mer NMR structure. For CS-A and heparin, it was necessary only to extend or truncate the structure to the appropriate length. We prepared CS-D and CS-E by extending the CS-A structure to a 12-mer, modifying the sulfation pattern, optimizing the side chains, and performing 5 ns of molecular dynamics (MD) in aqueous solution. MD system preparation and simulation parameters are further outlined in the supporting information. The structure closest to the average during MD was selected as the conformation for docking. This conformation was then truncated to a hexa- or octa-saccharide by removing sugars

from both the reducing and non-reducing ends. This step was necessary because the terminal saccharides display high variability in torsion angles during MD that are unphysical (inconsistent with possible movements) for an extended polysaccharide (5, 6).

All crystal structure ligands were prepared by identifying the appropriate DREIDING atom types and assigning Mulliken charges from Density Functional Theory (DFT) calculations [B3LYP flavor using the 6-311G** basis set) using Jaguar.

Heparin and CS ligands for the predicted systems (RPTPσ, NgR1, NgR2, and NgR3) were generated from available 18-mer heparin NMR structures (6) and a 6-mer CS-A (4) crystal structure as mentioned above. The heparin and CS-A structures were truncated or extended as needed for docking. Generating CS-D and CS-E required modifying the sulfation pattern of an extended 12-mer CS-A structure.

The sulfation pattern was modified using the Maestro software, Mulliken charges were calculated, and the MacroModel Conformational Search tool was used to sample the sidechain torsions (the sugar backbone was kept fixed). The resulting conformations were minimized using DREIDING and MPSim with Surface Generalized Born (SGB) solvation. The lowest-energy conformation was then selected for MD.

The AMBER package was used to place the 12-mer in a water box with a number of sodium ions added to neutralize the ligand charge. Dynamics was performed using NAMD (7) in four steps as described in the next section. Briefly, first, the water box was minimized with the ligand kept fixed. Second 0.5 ns of MD were performed on the water box. Third, the entire system was minimized. Finally, 5 ns of MD were performed on the entire system. The final ligand conformation for docking was the conformation closest to the average structure from the 5 ns MD. The 12-mer was truncated for docking by removing the terminal sugars. In addition, these MD trajectories were used to generate multiple ligand conformations for docking to sample conformational changes in the GAG backbone during docking. A ligand conformation was output for each MD step, and all conformations were clustered based on ligand RMSD into 12 groups. The lowest energy conformation from each group was used for docking.

GAG-Dock Summary:

We perform a two-step process for each GAG-protein complex, we first identify likely GAG binding sites on the target protein using coarse docking and then we re-dock using find docking to identify strongly bound poses.

In the first step, for “coarse-docking” we dock a single GAG conformation to the entire protein surface to identify likely binding sites. This configuration is chosen by minimizing the ligand in the solvent. Here, docking to the ‘alanized’ structure allows us to quickly scan the entire protein for putative GAG binding sites by optimizing the long-range Coulomb interactions.

In the second step, for “fine-grained” we re-dock to the best coarse regions to identify specific, strongly bound poses. In this step, we sample ligand conformations more completely allowing rotations about single bonds to accommodate the intrinsic flexibility of the GAG ligand. We selected 12 conformations to have low energies while remaining diverse, as described under ligand preparation. Then do rigid docking of this ensemble of 12 GAG ligand conformations. Finally, all final energies for all poses for all 12 conformations are ranked together by total energy and the best 100 are minimization before identifying the top docked structure for each GAG-protein complex. These methods are detailed further below and in the SI.

DarwinDock

The concept behind DarwinDock (8-13) is (1) to generate a complete set of poses for the binding site while minimizing the number of energy evaluations, (2) then to collect these into a smaller sets containing all poses likely to be important, (3) then to evaluate the binding energy of this relatively small set to find the best poses, while ensuring that no poses are missed that might prove to be important.

Pose generation is accomplished by iteratively generating poses (but no energies) using DOCK 6 (14) and clustering them into families using our Closest-Neighbor Seeded clustering algorithm (described below). Our usage of DOCK 6 is very simplistic, utilizing only the bump filter. We follow the default settings for generating the bump grid for DOCK 6 and set the bump cutoff to 5. Two calls to DOCK 6 are generally made. First, a request for 40,000 poses is made to determine the approximate percentage of poses that will pass the DOCK bump filter. Then a second request for poses is made, based on the percent of poses passing the bump test so that enough poses are returned to be sufficient for the iterative completeness cycle. Initially the first 5000 poses are clustered with a 2 Å diversity, then the next 5000 poses are added and reclustered, leading an increased number of families. This process is continued in increments of 5000 poses until the number of new families represents less than 5% of the total number of families at that point.

Due to the computational difficulty of dealing with GAG ligands – which are considerably larger than normal small-molecule ligands for which DarwinDock was developed – leading to correspondingly increased search volumes, we restrict the number of poses during this iterative completeness cycle to 50,000. Furthermore, it is generally not possible to request more than 15 million poses (sometimes fewer) from DOCK6 before memory-limitations intercede. As a result, most regions reach the 50,000 pose limit before reaching the 5% new families threshold. Other regions may fall well short of 50,000 poses due to their geometry and memory limitations.

After generating a complete set of poses, or the largest set within our computational limits, we score all family heads (generally ~2000). For each family the central pose (based on the RMSD) is denoted as the family head. The protein-ligand interaction energy of each family head is evaluated using the DREIDING forcefield with MPSim (15, 16). DREIDING partitions non-bond energies into Coulomb, hydrogen-bond, and van der Waals (vdW) contributions. For GAG-Dock the interaction energy is the sum of all ligand-protein Coulomb and hydrogen-bond energies plus 10% of the vdW energy. Including only 10% of the vdW energy allows for strong polar interactions with the protein with moderate clashes that can be resolved during side chain optimization. Not including the VDW energy results in poses with severe, unresolvable clashes with the protein, while including the full VDW energy results in poses that are too far from the protein and make poor contact.

After evaluating the interaction energy for the family heads, we eliminate the worst 90% of the families. Next, we evaluate the interaction energy for all children in the remaining 10% of families. From these children we select best 100 based on binding energy. Eliminating 90% of the families without evaluating all of their child poses allows for a large fraction of the complete set of poses to be eliminated without the time-consuming energy evaluation.

The 100 selected poses are then further refined with side chain optimization using SCREAM (17). Any side chain that was alanized prior to docking is now restored and optimized ("de-alanized") by SCREAM. Simultaneously, any polar or charged side chain in the binding site is also optimized by SCREAM, resulting in 100 unique sets of side chain conformations each adapted to a specific ligand pose. Each complex is then energy optimized for 10 steps of

conjugate gradient minimization. The minimized complexes are then scored using the "snap" binding energy, which is the total energy of the protein and the total energy of the ligand subtracted from the total energy of the complex, all calculated using DREIDING and MPSim. We then eliminated half of these complexes based on these energies. The remaining half was optimized with an additional 50 steps of conjugate gradient minimization. These fully-minimized complexes were rescored again, and the top one or two poses identified for analysis.

Closest-Neighbor Seeded Ligand Clustering

The Closest-Neighbor Seeded (CNS) ligand clustering algorithm uses a RMSD-based metric to cluster ligands into families and to assign family heads. First, all pairwise ligand RMSDs were calculated (ignoring hydrogen atoms). These pairwise RMSDs were placed in a list ordered from smallest RMSD to largest. The pair of ligands with the smallest RMSD constitutes the seed for the first family/cluster. Proceeding down the list of pairs *i* and *j*, the following operations were carried out:

1. If pose *i* and pose *j* do not belong to a pre-existing family, then a new family is seeded
2. If pose *i* belongs to family *A* and pose *j* does not (or *vice versa*):
   If the RMSD of pose *j* to all members of family *A* is less than the diversity RMSD, then pose *j* is added to family *A*
3. If pose *i* belongs to family *A* and pose *j* belongs to family *B*:
   If the RMSD of pose *i* to all members of family *B* is less than the diversity RMSD, and if the RMSD of pose *j* to all members of family *A* is less than the diversity RMSD, then the two families are merged into a single family

The pose with the lowest RMSD to the rest of the members is designated as the family head. If a family only has two members then the family head is chosen randomly.

Force Field

All force field calculations during docking – with the exception of sidechain optimizations – were performed using the DREIDING force field and the MPSim molecular dynamics code. DREIDING uses a three-body hydrogen bond term that allows a more precise analysis of the energetics. It also eliminates the need of SHAKE constraints that must be used with the 2-body hydrogen bonds used in most force fields.

Side Chain Optimization

Side chain optimization was performed using the SCREAM program (17) (using the DREIDING force field).

Sphere Generation

Spheres were generated using a modified *sphgen* program (14). Specifically, two sets of spheres were generated for each protein:

The "normal" set:

- Use a 1.4 Å probe radius in the *dms* molecular surface program
- Use dotlim=–0.9 in *sphgen*
- Use 1.4 Å minimum and 10 Å maximum sphere radii in *sphgen*

The "restriction" set:

- Use 2.8 Å probe radius in *dms*
- Use dotlim=–0.9' in *sphgen*
- Use 2.8 Å minimum and 10 Å maximum sphere radii in *sphgen*

The final set of spheres is taken from the "normal" set with the criteria that a sphere must be within 2.8 Å of a sphere from the "restriction" set.

The final set of spheres was partitioned into overlapping boxes having 20 Å sides and allowing 5 Å overlap.

As mentioned above, we assign electrostatic potential values to the spheres. The electrostatic potential for the protein is generated using APBS (18) and mapped onto the generated spheres. The electrostatic potential for a given sphere is taken from the value from the nearest APBS grid point.

Sphere Clustering

In order to reduce the number of spheres in each region to a computationally-manageable number, the spheres are clustered using the CNS algorithm, with each sphere treated as a single-atom ligand. The clustering diversity is set at 0.25 and increased until the total number of families is less than 150, or until the diversity is 3.00. For sphere families with 3 or more spheres, the family head is kept to represent the family. For sphere families of 2 spheres, the coordinates are averaged.

Molecular Dynamics (MD)

The MD simulations were carried out using NAMD, a parallel MD code designed for computationally demanding biomolecular systems. The CHARMM force field was used for the protein and ligands. The TIP3P force field was used for water. NAMD employs periodic boundary conditions to remove surface effects. The full electrostatic interactions within this periodic system is calculated using the particle-mesh Ewald summation method. The long-range electrostatic and van der Waals interactions were cut off at 12 Å (with spline smoothing).

The calculations were performed under isothermal-isobaric conditions (NPT) at 310 K and 1 atm. The temperature was controlled using Langevin dynamics (with a coupling coefficient of 5 ps^{-1}) and the pressure is maintained using a Langevin-Hoover barostat. A time step of 1 fs was used throughout this study.

Simulations. The MD is carried out in 4 steps:

a) The water atoms and counter-ions were conjugate gradient minimized for 5000 steps while keeping the protein and ligand atoms fixed. This allows for the water and counter ions to remove any bad contacts with each other and the protein or the ligand, prior to MD.

b) Then the water and counter ion atoms were equilibrated under NPT conditions (310 K and 1 atm) for 0.5 ns, while keeping the protein and ligand fixed. This allows the and waters and counter ions to equilibrate in the presence of the protein and to fill any gaps around the protein created due to system setup.

c) Next, the full system (protein-ligand-water) was minimized for 5000 steps, allowing the protein and ligand to adjust to the equilibrated water and counter ions.

d) Finally, the full system is equilibrated for at least 5 ns under NPT conditions, of which only the last 5 ns is used for dynamical analysis. Snapshots are saved every 1 ps.

Supporting References

1. D.A. Case W. Botello-Smith, D.S. Cerutti, T.E. Cheatham, III, T.A. Darden, R.E. Duke, T.J. Giese, H. Gohlke, A.W. Goetz, N. Homeyer, S. Izadi, P. Janowski, J. Kaus, A. Kovalenko, T.S. Lee, S. LeGrand, P. Li, C. Lin, T. Luchko, R. Luo, B. Madej, D. Mermel RMB (2016) AMBER. ((2016), AMBER 2016, University of California, San Francisco.).
2. Mayo SL, Olafson BD, Goddard WA (1990) DREIDING: a generic force field for molecular simulations. J phys Chem 94(26):8897–8909.
3. Kim DE, Chivian D, & Baker D (2004) Protein structure prediction and analysis using the Robetta server. Nucleic acids research 32(suppl_2):W526-W531.
4. Winter W, Arnott S, Isaac D, & Atkins E (1978) Chondroitin 4-sulfate: the structure of a sulfated glycosaminoglycan. Journal of molecular biology 125(1):1-19.
5. Tanaka K (1978) Physicochemical Properties of Chondroitin Sulfate: I. Ion Binding and Secondary Structure. The Journal of Biochemistry 83(3):647-653.
6. Khan S, Gor J, Mulloy B, & Perkins SJ (2010) Semi-rigid solution structures of heparin by constrained X-ray scattering modelling: new insight into heparin–protein complexes. Journal of molecular biology 395(3):504-521.
7. Phillips JC, et al. (2005) Scalable molecular dynamics with NAMD. J Comput Chem 26(16):1781–1802.
8. Floriano WB, Vaidehi N, Zamanakos G, & Goddard WA (2004) HierVLS hierarchical docking protocol for virtual ligand screening of large-molecule databases. Journal of medicinal chemistry 47(1):56-71.
9. Scott CE, Abrol R, Ahn KH, Kendall DA, & Goddard WA (2013) Molecular basis for dramatic changes in cannabinoid CB1 G protein- coupled receptor activation upon single and double point mutations. Protein Science 22(1):101-113.
10. Kirkpatrick A, Heo J, Abrol R, & Goddard WA (2012) Predicted structure of agonist-bound glucagon-like peptide 1 receptor, a class BG protein-coupled receptor. Proceedings of the National Academy of Sciences 109(49):19988-19993.
11. Charlier L, et al. (2012) How broadly tuned olfactory receptors equally recognize their agonists. Human OR1G1 as a test case. Cellular and molecular life sciences:1-9.
12. Kim SK, Riley L, Abrol R, Jacobson KA, & Goddard WA (2011) Predicted structures of agonist and antagonist bound complexes of adenosine A3 receptor. Proteins: Structure, Function, and Bioinformatics 79(6):1878-1897.
13. Kim S-K, Li Y, Abrol R, Heo J, & Goddard III WA (2011) Predicted structures and dynamics for agonists and antagonists bound to serotonin 5-HT2B and 5-HT2C receptors. Journal of chemical information and modeling 51(2):420-433.
15. Cho AE, et al. (2005) The MPSim- Dock hierarchical docking algorithm: Application to the eight trypsin inhibitor cocrystals. Journal of computational chemistry 26(1):48-71.
14. Allen WJ, et al. (2015) DOCK 6: Impact of new features and current docking performance. J Comput Chem 36(15):1132–1156.
16. Lim K-T, et al. (1997) Molecular dynamics for very large systems on massively parallel computers: the MPSim program. J Comput Chem 18(4):501–521.
17. Tak Kam VW & Goddard III WA (2008) Flat-bottom strategy for improved accuracy in protein side-chain placements. Journal of chemical theory and computation 4(12):2160-2169.
18. Dolinsky TJ, Nielsen JE, McCammon JA, Baker NA (2004) PDB2PQR: an automated pipeline for the setup of Poisson–Boltzmann electrostatics calculations. Nucleic Acids Res 32(suppl 2):W665–W667.

Supporting Figures

Figure S1 – Summary of docking validations for GAG-protein systems with available crystal structures. The resolution of the x-ray structure is given along with the heavy-atom RMSD between the predicted and x-ray position of the ligand

Figure S2 – Structure of FGF1 [PDB: 2AXM, resolution 3.00 Å] with predicted and crystal heparin hexamer ligands (magenta: predicted, green: crystal). Residues in the binding site with significant deviations from the crystal are labeled (cyan: predicted, orange: crystal). Ligand RMSD is 0.70 Å.

Figure S3 – Structure of FGF1 [PDB: 2AXM, res. 3.00 Å] with predicted heparin hexamer ligand (magenta) and 5 Å binding site shown (cyan). Dashed lines indicate hydrogen bonding and salt bridges between ligand and protein. The predicted ligand has excellent agreement with the crystal ligand, RMSD: 0.70 Å.

Figure S4 – Structure of FGF2 [PDB: 1BFB, res. 1.90 Å] with predicted heparin tetramer ligand (magenta) and 5 Å binding site shown (cyan). Dashed lines indicate hydrogen bonding and salt bridges between ligand and protein. The predicted ligand has excellent agreement with the crystal ligand, RMSD: 0.70 Å.

Figure S5 – Structure of FGF2-FGFR1 [PDB: 1FQ9, res. 3.00 Å] chain A with predicted heparin hexamer ligand (magenta) and 5 Å binding site shown (cyan). Dashed lines indicate hydrogen bonding and salt bridges between ligand and protein. The predicted ligand has excellent agreement with the crystal ligand, RMSD: 1.51/0.75 Å.

Figure S6 – Structure of FGF2-FGFR1 [PDB: 1FQ9, res. 3.00 Å] chain B with predicted heparin hexamer ligand (magenta) and 5 Å binding site shown (cyan). Dashed lines indicate hydrogen bonding and salt bridges between ligand and protein. The predicted ligand has excellent agreement with the crystal ligand, RMSD: 1.51/0.75 Å.

Figure S7 – Structure of FGF2-FGFR1 [PDB: 1FQ9, res. 3.00 Å] chain C with predicted heparin hexamer and octamer ligands (magenta) and 5 Å binding site shown (cyan). Dashed lines indicate hydrogen bonding and salt bridges between ligand and protein. The predicted ligand has excellent agreement with the crystal ligand, RMSD: 1.51/0.75 Å.

Figure S8 – Structure of FGF2-FGFR1 [PDB: 1FQ9, res. 3.00 Å] chain C with predicted heparin hexamer and octamer ligands (magenta) and 5 Å binding site shown (cyan). Dashed lines indicate hydrogen bonding and salt bridges between ligand and protein. The predicted ligand has excellent agreement with the crystal ligand, RMSD: 1.51/0.75 Å.

Figure S9 – Structure of α-antithrombin-III [PDB: 1E03, res. 2.90 Å] with predicted heparin analog pentamer ligand (magenta) and 5 Å binding site shown (cyan). Dashed lines indicate hydrogen bonding and salt bridges between ligand and protein. The predicted ligand has excellent agreement with the crystal ligand, RMSD: 0.60 Å.

Figure S10 - Plots of nonbond energies for residues in the (A) FGF1, (B) FGF2, (C) FGF2-FGFR1 Chain A complex, (D) FGF2-FGFR1 Chain B complex, and (E) α-Antithrombin-III binding sites in complex with a heparin ligand in the crystal versus docked structure. Residues with significant deviations from the trend are labeled.

Figure S11 – Per-residue energetic contributions in the FGF1/heparin predicted (left) and crystal (right) structures. [PDB: 2AXM, res. 3.00 Å, RMSD: 0.70 Å].

Figure S12 – Per-residue energetic contributions in the FGF2/heparin predicted (left) and crystal (right) structures. [PDB: 1BFB, res. 1.90 Å, RMSD: 0.70 Å].
Figure S13 – Per-residue energetic contributions in the FGF2-FGFR1/heparin predicted (left) and crystal (right) structures for chains A and B. [PDB: 1FQ9, res. 3.00 Å, RMSD: 1.51/0.75 Å].
Figure S14 – Per-residue energetic contributions in the FGF2-FGFR1/heparin-A predicted (left) and crystal (right) structures for chain C. [PDB: 1FQ9, res. 3.00 Å, RMSD: 1.51/0.75 Å].
Figure S15 – Per-residue energetic contributions in the FGF2-FGFR1/heparin-A predicted (left) and crystal (right) structures for chain D. [PDB: 1FQ9, res. 3.00 Å, RMSD: 1.51/0.75 Å].
Figure S16 – Per-residue energetic contributions in the FGF2-FGFR1/heparin-B predicted (left) and crystal (right) structures for chain C. [PDB: 1FQ9, res. 3.00 Å, RMSD: 1.51/0.75 Å].
Figure S17 – Per-residue energetic contributions in the FGF2-FGFR1/heparin-B predicted (left) and crystal (right) structures for chain D. [PDB: 1FQ9, res. 3.00 Å, RMSD: 1.51/0.75 Å].
Figure S18 – Per-residue energetic contributions in the Antithrombin-III/heparin analog predicted (left) and crystal (right) structures. [PDB: 1E03, res. 2.90 Å, RMSD: 0.60 Å].
Figure S19 – RPTPσ. (A) Ig1 and Ig2 domains of RPTPσ. (B) Electrostatic potential surface. (C-F) Predicted structures of CS-A, CS-D, CS-E, and heparin after docking and molecular dynamics.
Figure S20 – Predicted structure of CS-E hexamer (magenta) bound to RPTPσ with 5 Å binding site shown (cyan). Dashed lines indicate hydrogen bonding and salt bridges between ligand and protein.
Figure S21 – Predicted structure of heparin hexamer (magenta) bound to RPTPσ with 5 Å binding site shown (cyan). Dashed lines indicate hydrogen bonding and salt bridges between ligand and protein.
Figure S22 – Per-residue energetic contributions in the predicted RPTPσ/CS-A (left) and RPTPσ/CS-D (right) structures.
Figure S23 – Per-residue energetic contributions in the predicted RPTPσ/CS-E (left) and RPTPσ/heparin (right) structures.
Figure S24 – Electrostatic potential surfaces of (A) NgR1, (B) NgR2, and (C) NgR3. Note the lack of positive charge on NgR2, but strong positive charge on NgR1 and NgR3.
Figure S25 – NgR1. (A) Structure of NgR1. (B) Electrostatic potential surface showing strong positive charge. (C-F) Predicted structures of CS-A, CS-D, CS-E, and heparin after docking and molecular dynamics. (G-H) Detailed view of CS-E and heparin predicted structures.
Figure S26 – Detail of predicted NgR1/CS-A structure after docking and dynamics with CS-A hexamer (magenta) and 5 Å binding site (cyan) shown. Dashed lines indicate hydrogen bonding and salt bridges between ligand and protein. Overall placement on protein shown in inset.
Figure S27 – Detail of predicted NgR1/CS-D structure after docking and dynamics with CS-D hexamer (magenta) and 5 Å binding site (cyan) shown. Dashed lines indicate hydrogen bonding and salt bridges between ligand and protein. Overall placement on protein shown in inset.
Figure S28 – Detail of predicted NgR1/CS-E structure after docking and dynamics with CS-E hexamer (magenta) and 5 Å binding site (cyan) shown. Dashed lines indicate hydrogen bonding and salt bridges between ligand and protein. Overall placement on protein shown in inset.
Figure S29 – Detail of predicted NgR1/heparin structure after docking and dynamics with heparin hexamer (magenta) and 5 Å binding site (cyan) shown. Dashed lines indicate hydrogen bonding and salt bridges between ligand and protein. Overall placement on protein shown in inset.

Figure S30 – Per-residue energetic contributions in the predicted NgR1 structures for CS-A, CS-D, CS-E, and heparin.

Figure S31 – NgR3. (A) Structure of NgR3. (B) Electrostatic potential surface. (C-F) Predicted structures of CS-A, CS-D, CS-E, and heparin after docking and molecular dynamics. (G-H) Detailed view of CS-E and heparin predicted structures.

Figure S32 – Detail of predicted NgR3/CS-A structure after docking and dynamics with CS-A hexamer (magenta) and 5 Å binding site (cyan) shown. Dashed lines indicate hydrogen bonding and salt bridges between ligand and protein. Overall placement on protein shown in inset.

Figure S33 – Detail of predicted NgR3/CS-D structure after docking and dynamics with CS-D hexamer (magenta) and 5 Å binding site (cyan) shown. Dashed lines indicate hydrogen bonding and salt bridges between ligand and protein. Overall placement on protein shown in inset.

Figure S34 – Detail of predicted NgR3/CS-E structure after docking and dynamics with CS-E hexamer (magenta) and 5 Å binding site (cyan) shown. Dashed lines indicate hydrogen bonding and salt bridges between ligand and protein. Overall placement on protein shown in inset.

Figure S35 – Detail of predicted NgR3/heparin structure after docking and dynamics with heparin hexamer (magenta) and 5 Å binding site (cyan) shown. Dashed lines indicate hydrogen bonding and salt bridges between ligand and protein. Overall placement on protein shown in inset.

Figure S36 – Per-residue energetic contributions in the predicted NgR3 structures for CS-A, CS-D, CS-E, and heparin.

Figure S37 – Predicted sets of mutations to either increase (left) or decrease (right) binding of ligands to RPTPσ. Note that none of the sets show improved binding for heparin. Changes in binding energy are shown relative to the wild-type structures in both absolute change (kcal/mol) and in terms of percent change.

Figure S38 – Single residue mutation data for RPTPs. Values show change in binding energy (kcal/mol) relative to wild-type structures. Values are shown both for the change in hydrogen bonding for the specific mutated residue as well as the overall change in the full cavity binding energy. The cavity binding energy is further separated into hydrogen bonding + van der Waals or Coulomb energy.

Figure S39 – Predicted sets of mutations to either increase (left) or decrease (right) binding of ligands to NgR1. Note that none of the sets show improved binding for CS-E. Changes in binding energy are shown relative to the wild-type structures in both absolute change in binding energy (kcal/mol) and in terms of percent change.

Figure S40 – Single residue mutation data for NgR1. Values show change in binding energy (kcal/mol) relative to wild-type structures. Values are shown both for the change in hydrogen bonding for the specific mutated residue as well as the overall change in the full cavity binding energy. The cavity binding energy is further separated into hydrogen bonding + van der Waals or Coulomb energy.

Figure S41 – Predicted sets of mutations to either increase (left) or decrease (right) binding of ligands to NgR3. Changes in binding energy are shown relative to the wild-type structure in both absolute change (kcal/mol) and in terms of percent change.

Figure S42 – Single residue mutation data for NgR3. Values show change in binding energy (kcal/mol) relative to wild-type structures. Values are shown both for the change in hydrogen bonding for the specific mutated residue as well as the overall change in the full cavity binding energy. The cavity binding energy is further separated into hydrogen bonding + van der Waals or Coulomb energy.

	PDB	Resolution (Å)	RMSD* (Å)
FGF1	2AXM	3.00	0.70
FGF2	1BFB	1.90	0.70
FGF2-FGFR1 A	1FQ9	3.00	1.51
FGF2-FGFR1 B			0.75
α-ATIII	1EO3	2.90	0.60

*RMSD between docked and crystal structures

Figure S1 – Summary of docking validations for GAG-protein systems with available crystal structures. The resolution of the x-ray structure is given along with the heavy-atom RMSD between the predicted and x-ray position of the ligand

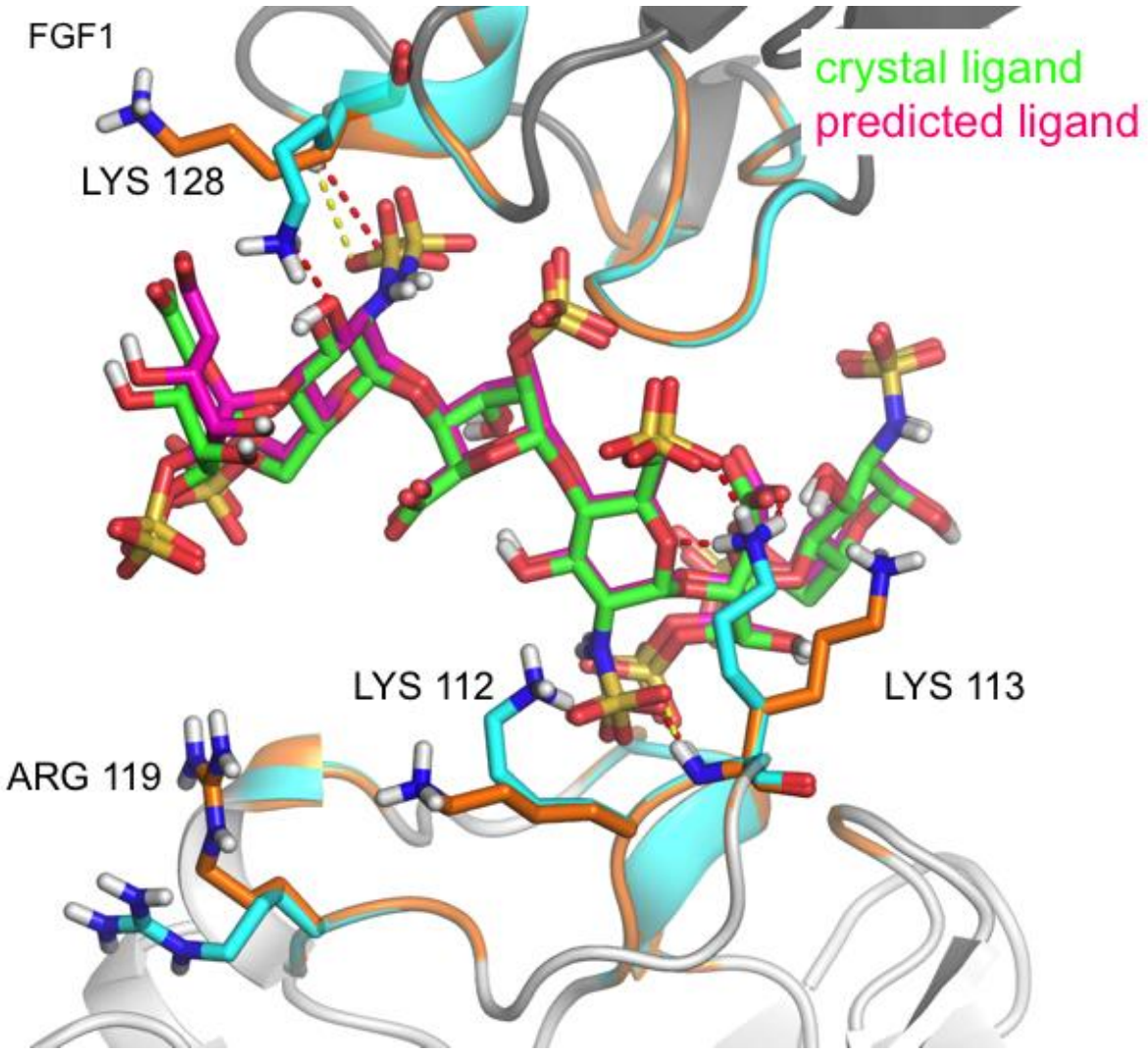

Figure S2 – Structure of FGF1 [PDB: 2AXM, resolution 3.00 Å] with predicted and crystal heparin hexamer ligands (magenta: predicted, green: crystal). Residues in the binding site with significant deviations from the crystal are labeled (cyan: predicted, orange: crystal). Ligand RMSD is 0.70 Å. See also: Figure 2, S3, S10, and S11.

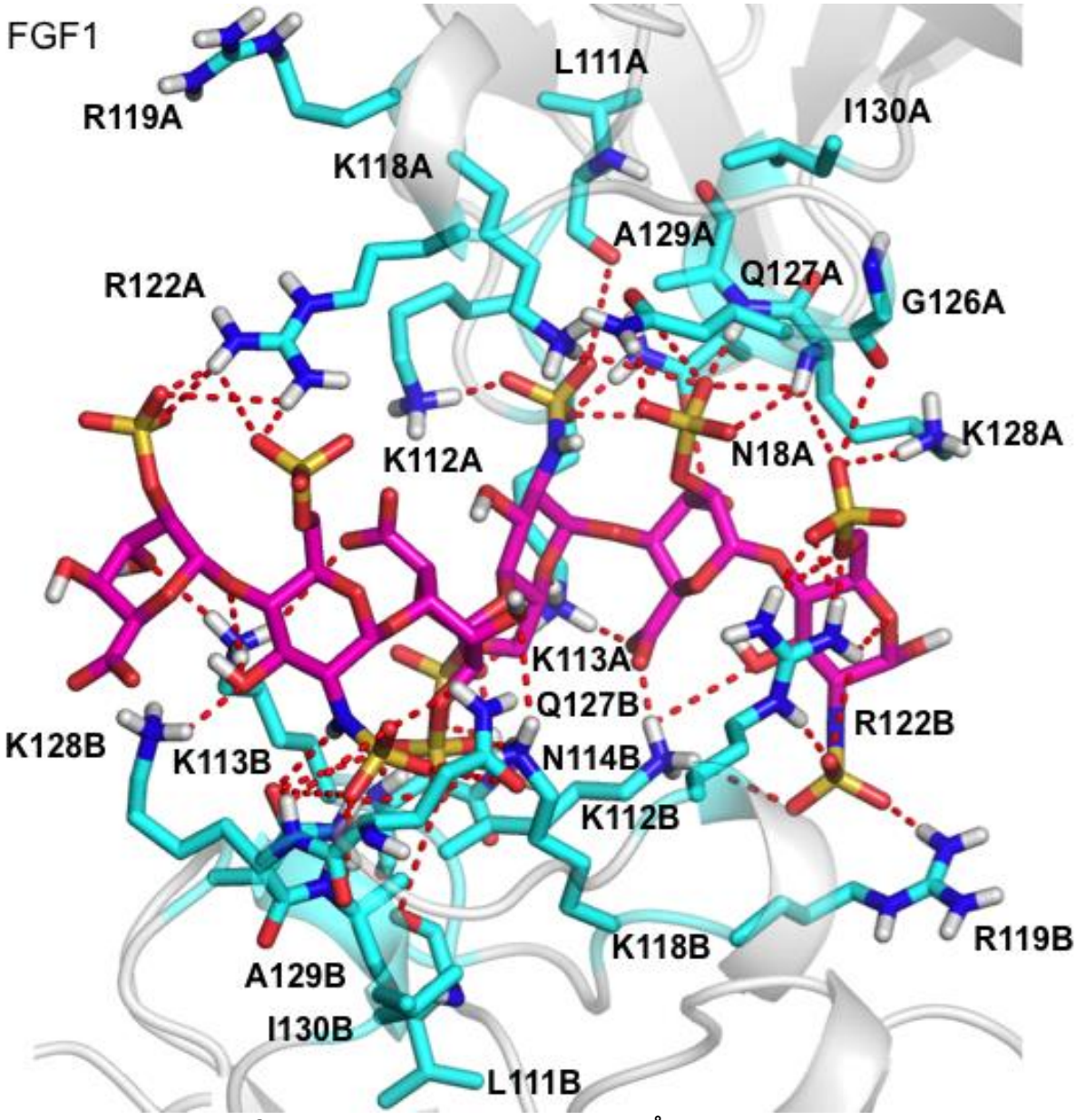

Figure S3 – Structure of FGF1 [PDB: 2AXM, res. 3.00 Å] with predicted heparin hexamer ligand (magenta) and 5 Å binding site shown (cyan). Dashed lines indicate hydrogen bonding and salt bridges between ligand and protein. The predicted ligand has excellent agreement with the crystal ligand, RMSD: 0.70 Å. See also: Figure 2, S2, S10, and S11.

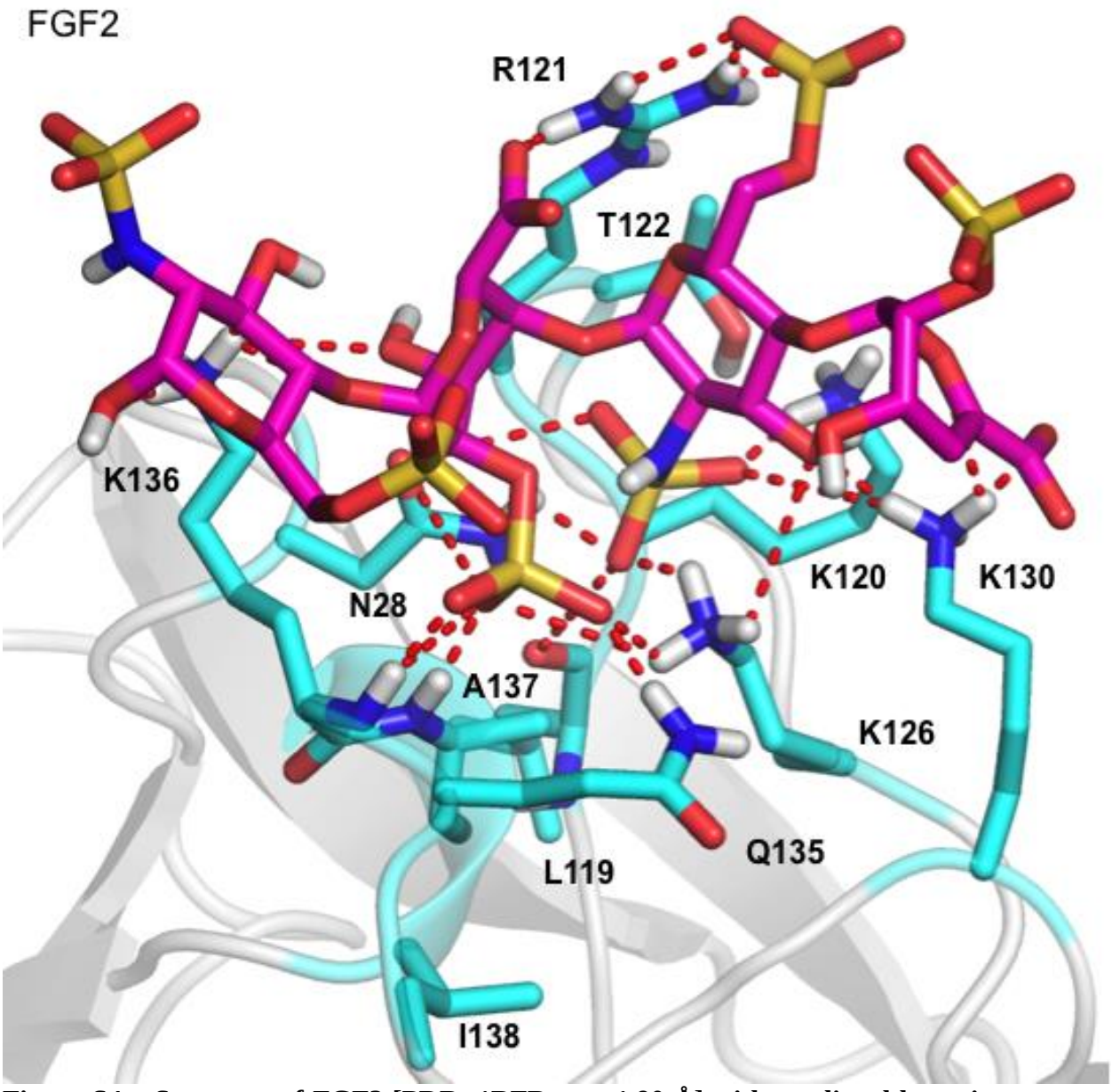

Figure S4 – Structure of FGF2 [PDB: 1BFB, res. 1.90 Å] with predicted heparin tetramer ligand (magenta) and 5 Å binding site shown (cyan). Dashed lines indicate hydrogen bonding and salt bridges between ligand and protein. The predicted ligand has excellent agreement with the crystal ligand, RMSD: 0.70 Å. See also: Figure 2, S10, and S12.

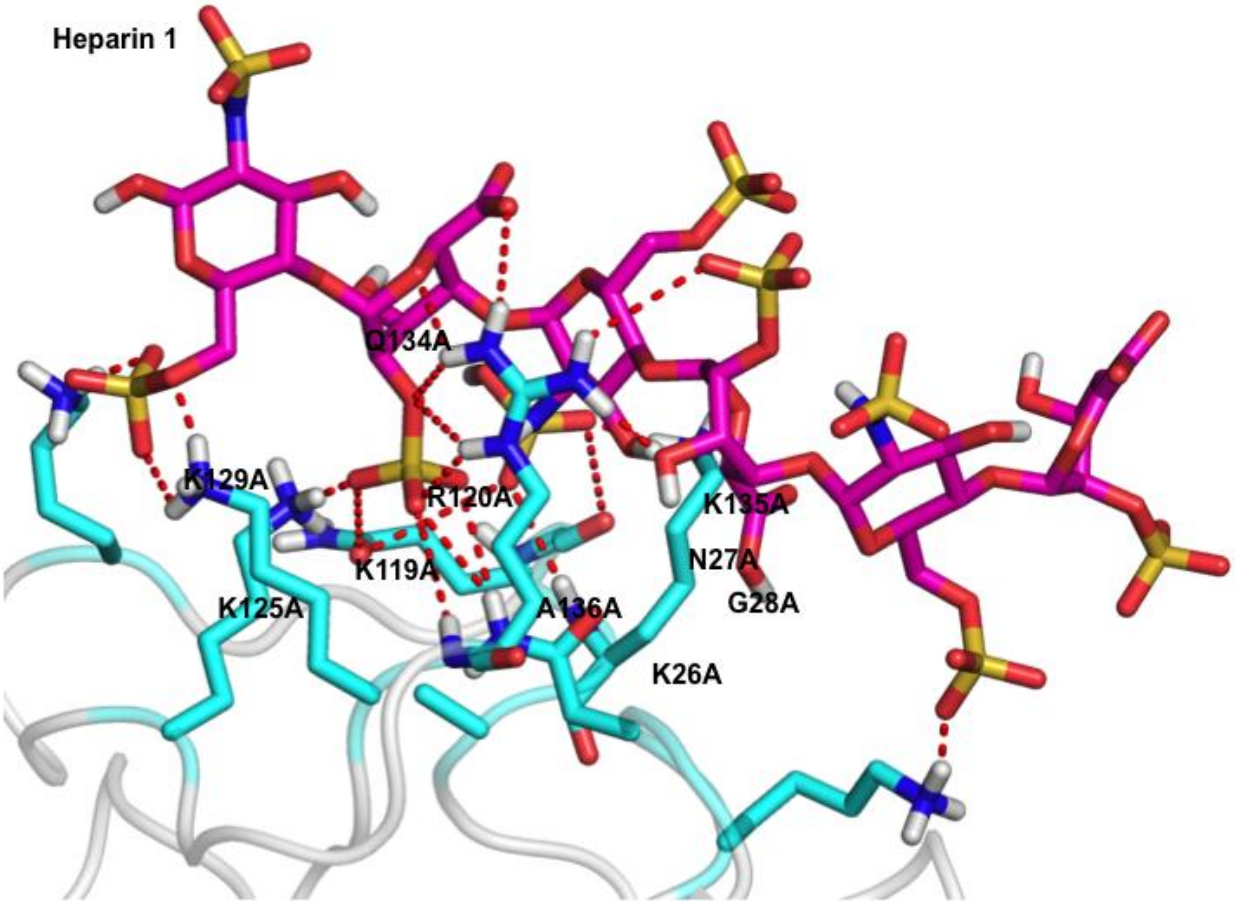

Figure S5 – Structure of FGF2-FGFR1 [PDB: 1FQ9, res. 3.00 Å] chain A with predicted heparin hexamer ligand (magenta) and 5 Å binding site shown (cyan). Dashed lines indicate hydrogen bonding and salt bridges between ligand and protein. The predicted ligand has excellent agreement with the crystal ligand, RMSD: 1.51/0.75 Å. See also: Figure 2, S6-S8, S10, and S13-S17.

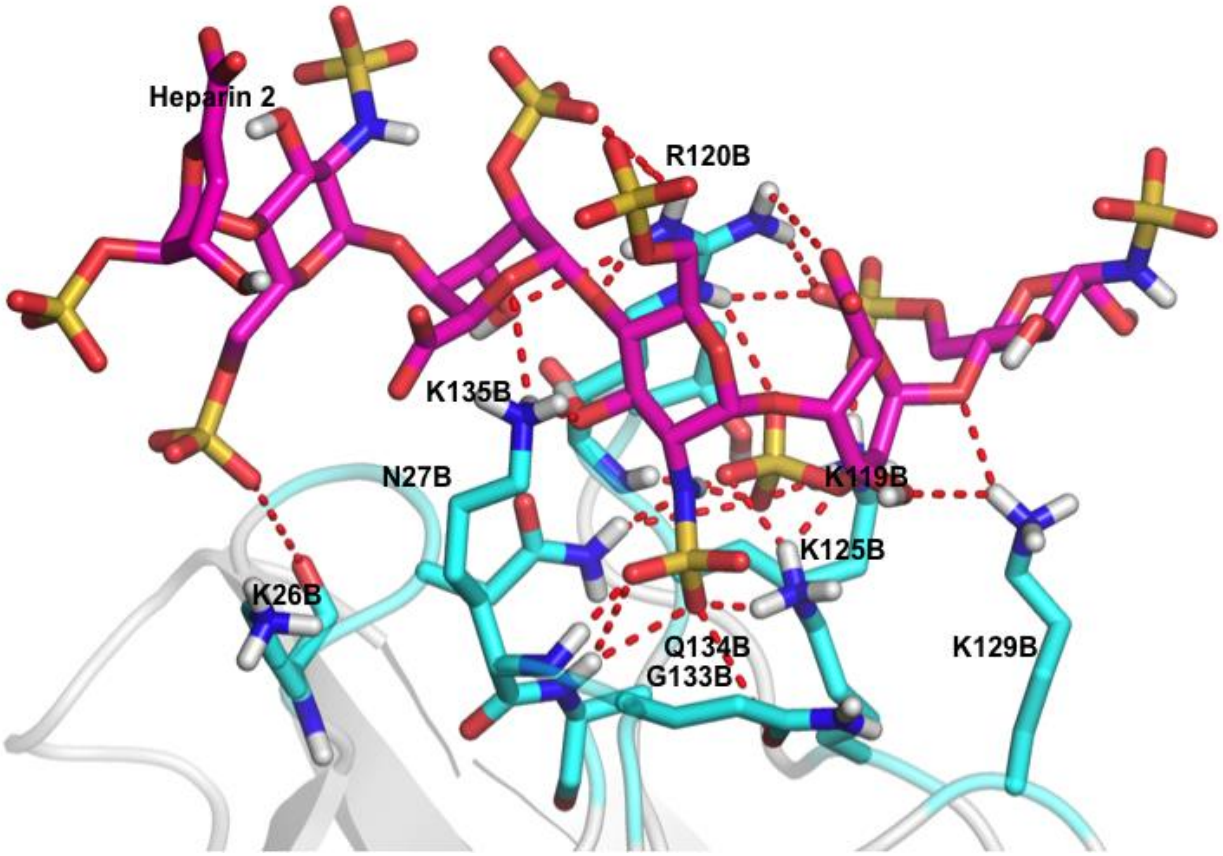

Figure S6 – Structure of FGF2-FGFR1 [PDB: 1FQ9, res. 3.00 Å] chain B with predicted heparin hexamer ligand (magenta) and 5 Å binding site shown (cyan). Dashed lines indicate hydrogen bonding and salt bridges between ligand and protein. The predicted ligand has excellent agreement with the crystal ligand, RMSD: 1.51/0.75 Å. See also: Figure 2, S5, S7-S8, S10, and S13-S17.

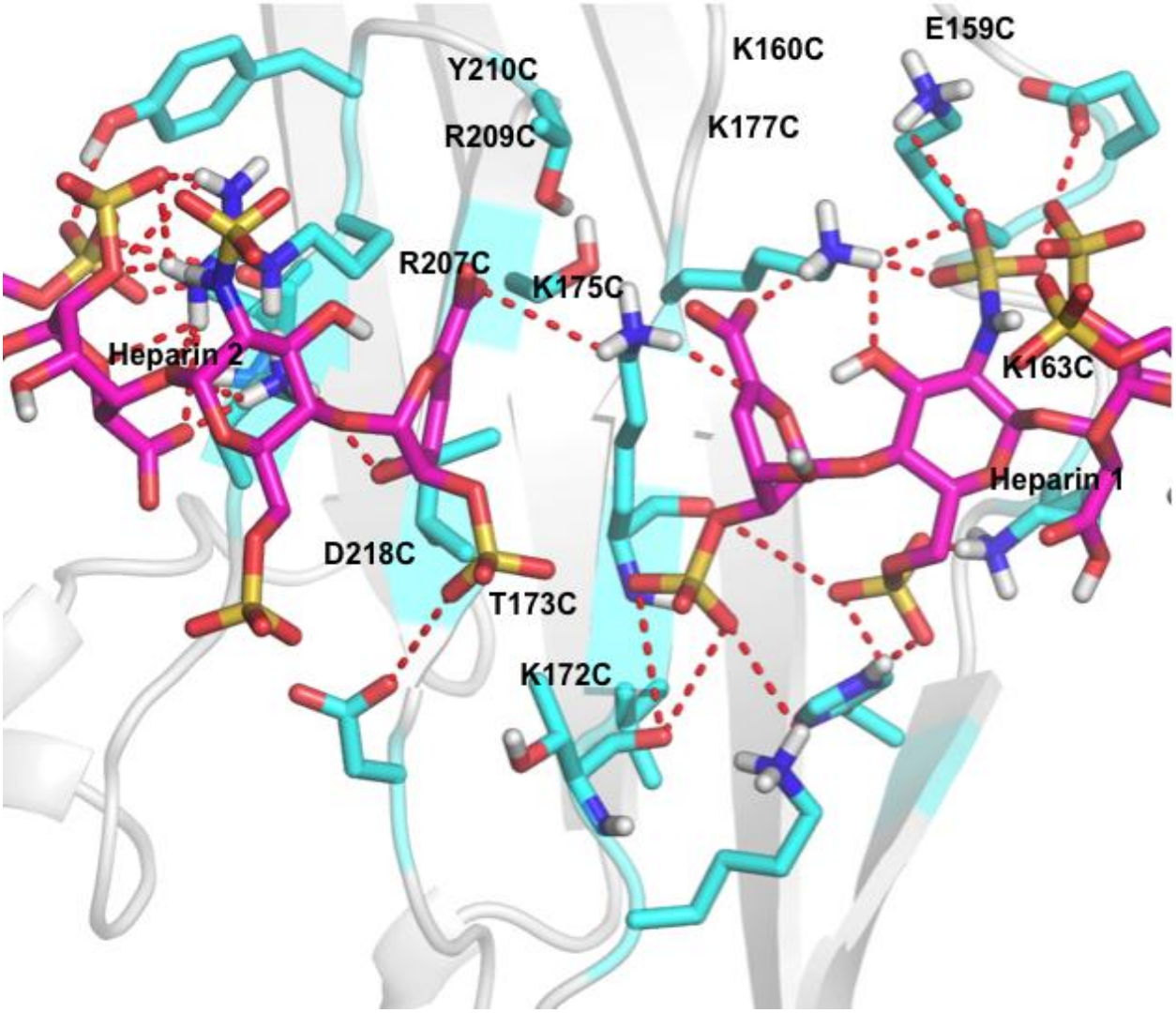

Figure S7 – Structure of FGF2-FGFR1 [PDB: 1FQ9, res. 3.00 Å] chain C with predicted heparin hexamer and octamer ligands (magenta) and 5 Å binding site shown (cyan). Dashed lines indicate hydrogen bonding and salt bridges between ligand and protein. The predicted ligand has excellent agreement with the crystal ligand, RMSD: 1.51/0.75 Å. See also: Figure 2, S5-S6, S8, S10, and S13-S17.

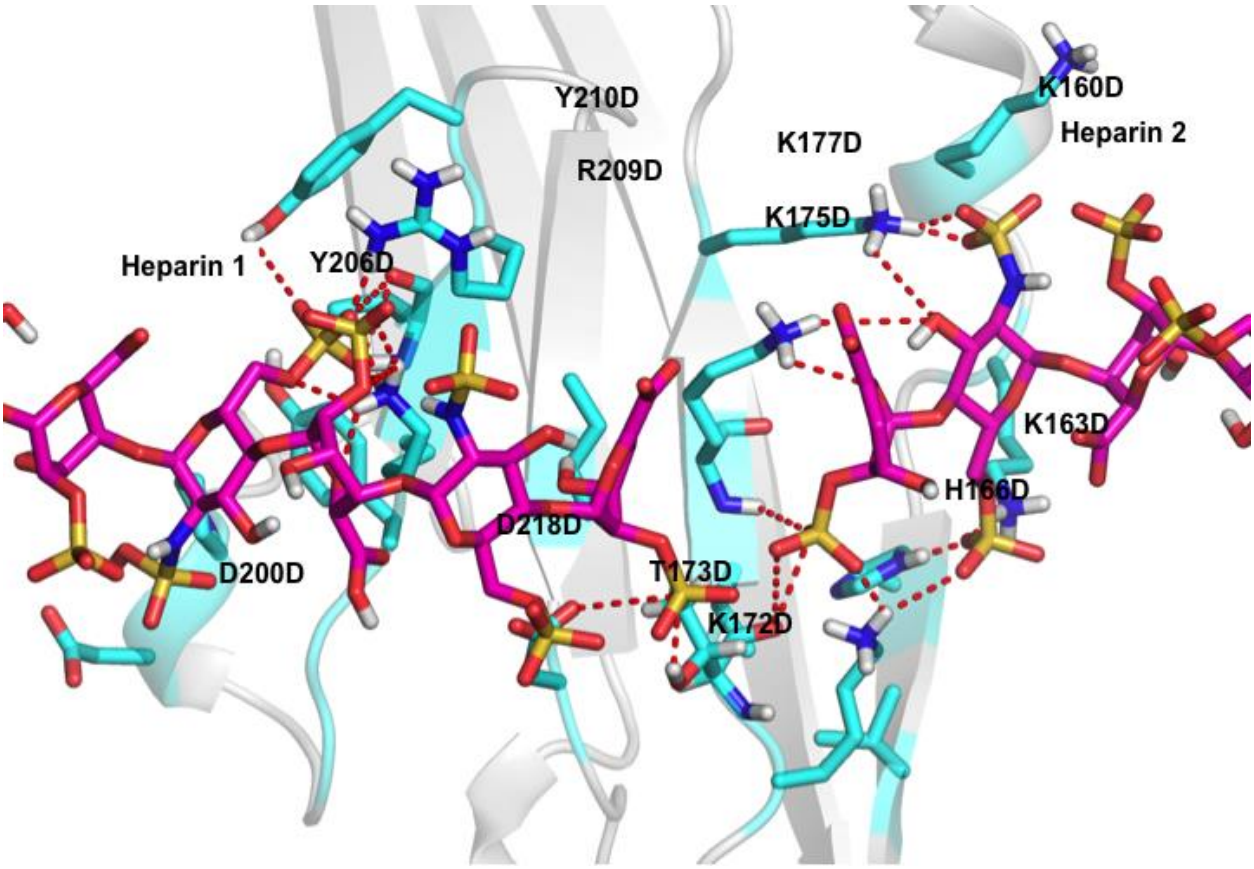

Figure S8 – Structure of FGF2-FGFR1 [PDB: 1FQ9, res. 3.00 Å] chain C with predicted heparin hexamer and octamer ligands (magenta) and 5 Å binding site shown (cyan). Dashed lines indicate hydrogen bonding and salt bridges between ligand and protein. The predicted ligand has excellent agreement with the crystal ligand, RMSD: 1.51/0.75 Å. See also: Figure 2, S5-S7, S10, and S13-S17.

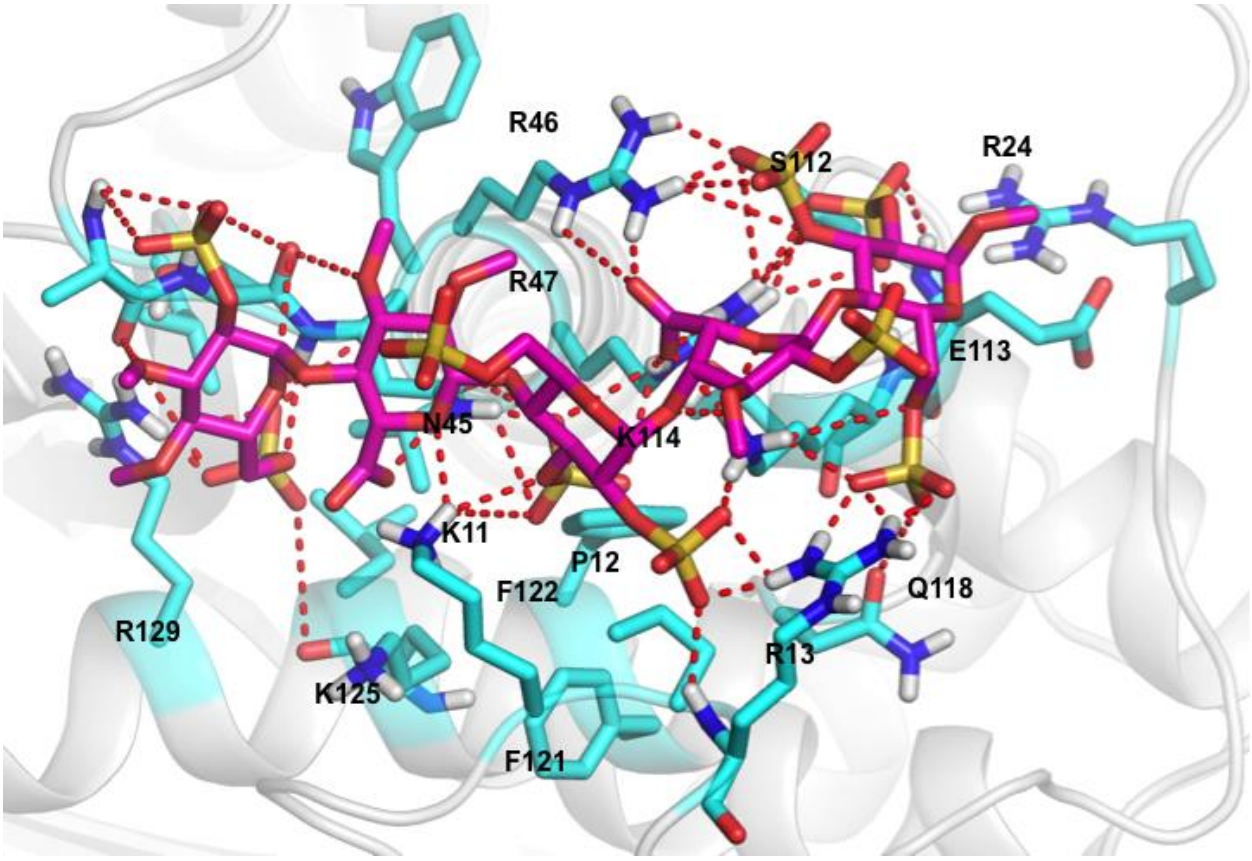

Figure S9 – Structure of α-Antithrombin-III [PDB: 1E03, res. 2.90 Å] with predicted heparin analog pentamer ligand (magenta) and 5 Å binding site shown (cyan). Dashed lines indicate hydrogen bonding and salt bridges between ligand and protein. The predicted ligand has excellent agreement with the crystal ligand, RMSD: 0.60 Å. See also: Figure 2, S10, and S16.

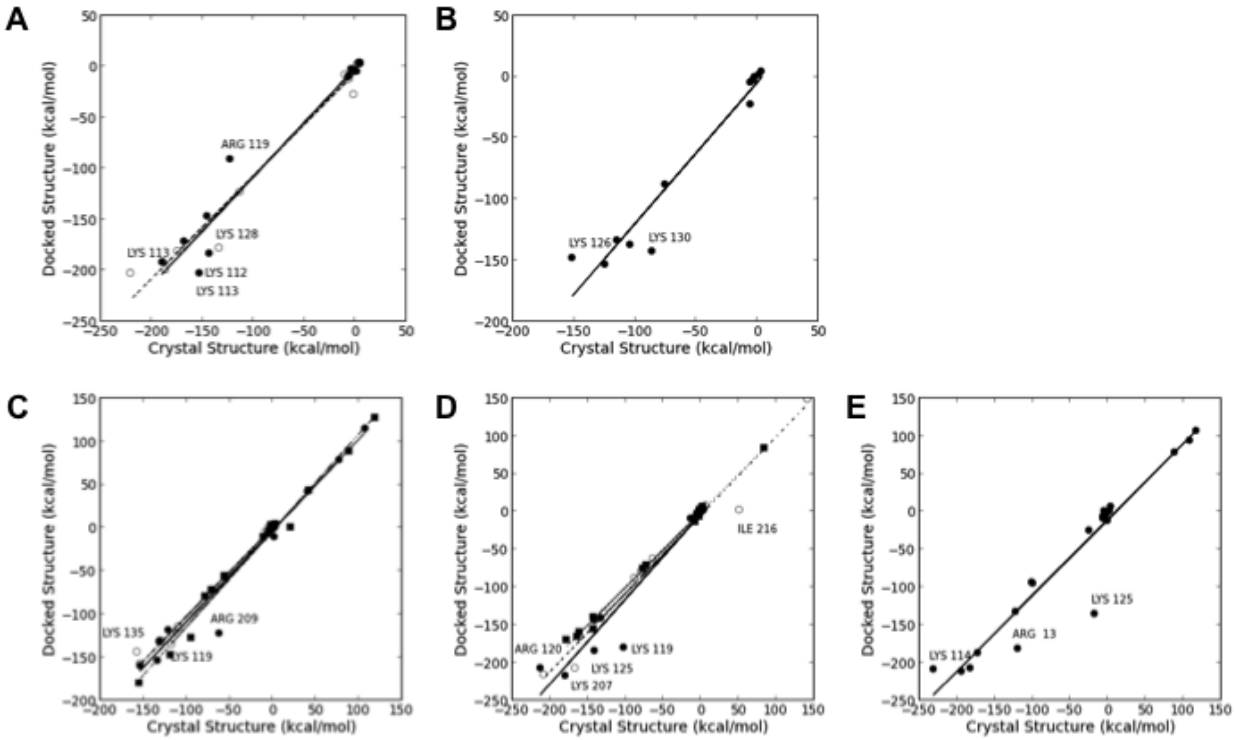

Figure S10 - Plots of nonbond energies for residues in the (A) FGF1, (B) FGF2, (C) FGF2-FGFR1 Chain A complex, (D) FGF2-FGFR1 Chain B complex, and (E) α-Antithrombin-III binding sites in complex with a heparin ligand in the crystal versus docked structure. Residues with significant deviations from the trend are labeled.

		Docked				Crystal				
	Residue	VdW	Coulomb	H Bond	NonBond	VdW	Coulomb	H Bond	NonBond	$\Delta_{NonBond}$
Chain A	LYS 113	17.56	-204.76	-15.75	-202.95	2.77	1.19	-2.00	1.96	-204.91
	LYS 118	3.22	-189.23	-5.96	-191.97	-0.56	4.09	0.00	3.54	-195.51
	LYS 112	3.29	-183.50	-3.81	-184.01	-0.33	-143.67	0.00	-144.00	-40.01
	ARG 122	7.16	-169.14	-9.33	-171.31	3.14	-153.18	-3.12	-153.17	-18.14
	LYS 128	3.06	-148.57	-1.85	-147.37	-0.41	4.77	0.00	4.37	-151.74
	ARG 119	-0.11	-91.00	0.00	-91.11	-0.06	-3.21	0.00	-3.27	-87.84
	GLN 127	-2.00	-8.03	0.00	-10.03	-1.99	-186.44	-1.59	-190.03	180.00
	ALA 129	5.47	-10.00	-4.60	-9.14	-0.38	-122.47	0.00	-122.86	113.72
	ASN 18	2.01	-1.44	-5.71	-5.13	-1.52	-165.54	-1.67	-168.72	163.59
	ILE 130	-0.32	-3.07	0.00	-3.39	-0.88	5.58	0.00	4.70	-8.08
	GLY 115	-0.04	-3.22	0.00	-3.27	-0.13	-6.95	0.00	-7.08	3.81
	GLY 126	-0.87	3.54	0.00	2.66	-4.08	-140.24	-1.57	-145.89	148.55
	LEU 111	-0.48	3.51	0.00	3.03	3.28	-8.41	-1.05	-6.18	9.21
	ASN 114	-0.23	3.33	0.00	3.10	-0.30	-2.97	0.00	-3.28	6.38
Chain B	LYS 113	4.89	-197.61	-9.67	-202.39	1.11	-215.76	-5.84	-220.49	18.10
	LYS 112	4.24	-198.73	-5.46	-199.96	2.69	-190.94	-0.44	-188.69	-11.26
	LYS 118	11.00	-197.81	-5.73	-192.53	-4.61	-181.97	0.00	-186.58	-5.96
	ARG 122	4.88	-176.18	-10.38	-181.68	2.69	-175.17	-1.89	-174.37	-7.31
	LYS 128	10.38	-181.92	-6.98	-178.52	2.06	-135.42	0.00	-133.36	-45.16
	ARG 119	7.42	-125.16	-5.83	-123.58	-2.11	-111.44	0.00	-113.55	-10.03
	ASN 114	5.11	-22.15	-10.47	-27.51	-0.34	-7.68	-1.92	-9.94	-17.57
	GLN 127	2.94	-13.43	-1.56	-12.05	-0.60	-5.77	0.00	-6.37	-5.68
	ALA 129	6.73	-10.22	-4.49	-7.99	-0.14	-3.90	0.00	-4.04	-3.94
	GLY 115	-0.14	-4.03	0.00	-4.17	-0.27	-2.84	0.00	-3.11	-1.07
	ILE 130	-0.37	-3.13	0.00	-3.50	-1.63	2.88	-3.24	-1.99	-1.50
	ASN 18	0.24	2.05	-5.05	-2.76	-2.38	1.24	-0.18	-1.32	-1.44
	GLY 126	-0.24	2.42	0.00	2.18	-0.56	2.92	0.00	2.36	-0.17
	LEU 111	-0.72	2.97	0.00	2.25	-0.25	2.86	0.00	2.61	-0.36

Figure S11 – Per-residue energetic contributions in the FGF1/heparin predicted (left) and crystal (right) structures. [PDB: 2AXM, res. 3.00 Å, RMSD: 0.70 Å]. See also: Figure 2, S2, S3, and S10.

		Docked				Crystal				
	Residue	**VdW**	**Coulomb**	**H Bond**	**NonBond**	**VdW**	**Coulomb**	**H Bond**	**NonBond**	$\Delta_{NonBond}$
Chain A	ARG 121	17.30	-158.68	-12.19	-153.56	-0.27	-150.23	-0.96	-151.45	-2.11
	LYS 126	9.10	-156.65	-0.36	-147.92	-3.44	-119.39	-2.31	-125.14	-22.78
	LYS 130	10.15	-144.73	-8.56	-143.15	-5.00	-107.74	-1.75	-114.49	-28.65
	LYS 120	8.16	-140.09	-5.58	-137.52	-2.88	-101.57	0.00	-104.45	-33.07
	LYS 136	6.73	-135.14	-5.78	-134.19	-0.75	-85.16	0.00	-85.91	-48.28
	LYS 27	-0.42	-87.54	0.00	-87.96	-0.28	-75.32	0.00	-75.60	-12.37
	GLN 135	2.17	-18.79	-6.09	-22.72	-2.77	-2.99	0.00	-5.76	-16.96
	ALA 137	7.94	-9.51	-3.59	-5.16	5.61	-8.31	-2.66	-5.37	0.21
	ILE 138	-0.28	-2.34	0.00	-2.62	-2.44	1.25	-1.53	-2.72	0.10
	ASN 28	3.07	-1.79	-3.76	-2.47	-0.28	-2.29	0.00	-2.57	0.10
	THR 122	-0.40	0.02	0.00	-0.37	-0.31	-1.32	0.00	-1.63	1.26
	GLY 134	-0.37	2.18	0.00	1.81	-0.43	2.34	0.00	1.92	-0.11
	LEU 119	-0.62	4.44	0.00	3.82	-0.45	4.03	0.00	3.57	0.25

Figure S12 – Per-residue energetic contributions in the FGF2/heparin predicted (left) and crystal (right) structures. [PDB: 1BFB, res. 1.90 Å, RMSD: 0.70 Å]. See also: Figure 2, S4, and S10.

		Docked				Crystal				
	Residue	VdW	Coulomb	H Bond	NonBond	VdW	Coulomb	H Bond	NonBond	$\Delta_{NonBond}$
Chain A	ARG 120	-2.28	-149.49	-5.26	-157.04	1.52	-152.06	-7.27	-157.81	0.77
	LYS 135	1.54	-139.58	-5.91	-143.95	4.60	-153.99	-3.79	-153.18	9.24
	LYS 119	0.67	-131.00	-4.78	-135.12	3.14	-130.93	-0.25	-128.04	-7.08
	LYS 125	5.84	-131.09	-5.87	-131.11	0.62	-116.95	-0.65	-116.98	-14.13
	LYS 26	4.39	-120.65	-5.68	-121.94	-1.02	-109.45	0.00	-110.47	-11.47
	LYS 129	4.99	-114.65	-5.58	-115.25	-1.24	-107.92	-0.68	-109.84	-5.41
	ALA 136	-0.53	-3.71	0.00	-4.24	2.86	-6.00	-4.60	-7.74	3.51
	GLY 28	-0.37	-2.08	0.00	-2.45	-2.02	1.97	-3.62	-3.67	1.22
	ILE 137	-0.12	-1.95	0.00	-2.07	-0.66	-1.95	0.00	-2.61	0.53
	GLN 134	-1.91	0.68	0.00	-1.23	-0.29	-2.08	0.00	-2.36	1.14
	ASN 27	-1.89	2.20	0.00	0.31	-0.48	-1.59	0.00	-2.08	2.39
	THR 121	-0.20	0.54	0.00	0.34	-0.17	-1.53	0.00	-1.70	2.04
	TYR 24	-0.14	1.63	0.00	1.49	4.63	-4.77	0.00	-0.14	1.63
	LEU 118	-0.15	2.35	0.00	2.20	-0.31	2.16	0.00	1.85	0.35
	GLY 133	-0.32	2.55	0.00	2.23	-0.50	2.69	0.00	2.19	0.04
	LEU 126	-0.14	2.56	0.00	2.42	-0.28	2.62	0.00	2.34	0.08
Chain B	LYS 135	1.19	-212.03	-6.46	-217.30	-8.49	-203.03	-1.48	-212.99	-4.31
	ARG 120	-6.58	-199.88	-1.36	-207.81	31.40	-208.27	-3.53	-180.39	-27.41
	LYS 125	5.60	-182.56	-6.84	-183.80	38.12	-175.56	-3.61	-141.05	-42.75
	LYS 119	12.36	-181.40	-10.45	-179.49	-2.14	-138.68	0.00	-140.82	-38.67
	LYS 129	-1.92	-141.31	-0.25	-143.48	-1.59	-130.86	0.00	-132.44	-11.04
	LYS 26	-2.18	-138.89	0.00	-141.07	37.15	-138.94	0.00	-101.78	-39.29
	GLN 134	-2.27	-6.73	0.00	-9.00	9.71	-20.50	-3.13	-13.92	4.92
	ALA 136	-1.24	-7.10	0.00	-8.34	-1.58	-6.76	0.00	-8.33	-0.01
	GLY 28	-0.34	-3.40	0.00	-3.74	-0.40	-2.89	0.00	-3.29	-0.45
	THR 121	-1.70	2.18	0.00	0.48	-0.16	-1.81	0.00	-1.97	2.44
	ASN 27	-2.39	4.25	0.00	1.86	3.82	-3.11	-0.03	0.68	1.18
	TYR 24	-0.15	2.25	0.00	2.10	-2.71	5.94	-0.05	3.18	-1.08
	GLY 133	-0.21	3.30	0.00	3.09	-0.25	3.55	0.00	3.30	-0.22
	LEU 118	-0.33	3.65	0.00	3.32	-0.52	3.96	0.00	3.44	-0.12

Figure S13 – Per-residue energetic contributions in the FGF2-FGFR1/heparin predicted (left) and crystal (right) structures for chains A and B. [PDB: 1FQ9, res. 3.00 Å, RMSD: 1.51/0.75 Å]. See also: Figure 2, S5-S8, S10, and S14-S17.

		Docked				Crystal				
	Residue	VdW	Coulomb	H Bond	NonBond	VdW	Coulomb	H Bond	NonBond	$\Delta_{NonBond}$
Chain C	LYS 177	7.03	-159.17	-8.16	-160.30	5.72	-158.41	-1.26	-153.95	-6.35
	LYS 175	0.73	-149.86	-4.69	-153.82	2.31	-130.03	-5.88	-133.60	-20.22
	LYS 163	6.37	-132.42	-6.11	-132.16	1.23	-132.09	-0.39	-131.25	-0.91
	LYS 160	0.37	-131.48	0.00	-131.12	-1.30	-129.72	-0.02	-131.03	-0.08
	ARG 209	-0.44	-117.34	-4.40	-122.18	-0.82	-120.14	0.00	-120.97	-1.21
	LYS 172	-0.78	-118.38	0.00	-119.16	-0.04	-70.04	0.00	-70.08	-49.08
	LYS 207	-0.04	-71.70	0.00	-71.75	-0.04	-61.48	0.00	-61.53	-10.22
	HSE 166	5.52	-12.11	-4.86	-11.44	-1.33	-3.41	0.00	-4.74	-6.70
	VAL 174	-0.99	-3.05	0.00	-4.04	-0.41	-2.90	0.00	-3.30	-0.74
	ILE 216	-0.52	-3.02	0.00	-3.54	-0.02	-1.90	0.00	-1.92	-1.62
	SER 219	-0.02	-1.90	0.00	-1.92	-0.02	-1.66	0.00	-1.68	-0.24
	TYR 206	-0.02	-1.58	0.00	-1.60	-0.01	-0.82	0.00	-0.83	-0.76
	VAL 208	-0.02	-0.86	0.00	-0.87	0.00	0.29	0.00	0.29	-1.16
	PRO 199	0.00	0.24	0.00	0.24	0.00	1.09	0.00	1.09	-0.85
	THR 173	-1.59	2.37	0.00	0.79	0.00	1.64	0.00	1.64	-0.85
	GLY 204	0.00	1.13	0.00	1.13	-1.28	3.00	0.00	1.72	-0.59
	GLY 205	0.00	1.63	0.00	1.63	-1.73	3.49	0.00	1.76	-0.13
	TYR 210	-0.02	2.19	0.00	2.18	-0.01	1.86	0.00	1.84	0.33
	ASP 200	0.00	41.39	0.00	41.39	0.00	41.11	0.00	41.10	0.28
	ASP 218	-0.09	78.09	0.00	78.01	-0.08	77.16	0.00	77.08	0.93
	GLU 159	-0.71	115.33	0.00	114.62	-0.45	107.49	0.00	107.04	7.59

Figure S14 – Per-residue energetic contributions in the FGF2-FGFR1/heparin-A predicted (left) and crystal (right) structures for chain C. [PDB: 1FQ9, res. 3.00 Å, RMSD: 1.51/0.75 Å]. See also: Figure 2, S5-S8, S10, S13, and S15-S17.

		Docked				Crystal				
	Residue	VdW	Coulomb	H Bond	NonBond	VdW	Coulomb	H Bond	NonBond	$\Delta_{NonBond}$
Chain D	LYS 207	7.45	-180.81	-6.56	-179.92	17.13	-171.90	-0.35	-155.12	-24.79
	ARG 209	3.65	-146.18	-5.18	-147.70	-0.83	-117.34	0.00	-118.16	-29.54
	LYS 175	5.98	-126.60	-6.24	-126.87	-0.40	-94.29	0.00	-94.69	-32.18
	LYS 172	-0.12	-79.28	0.00	-79.40	-0.12	-78.00	0.00	-78.11	-1.29
	LYS 177	-0.04	-72.16	0.00	-72.20	-0.03	-70.11	0.00	-70.14	-2.06
	LYS 160	-0.01	-56.66	0.00	-56.66	0.00	-55.42	0.00	-55.42	-1.25
	LYS 163	-0.01	-56.16	0.00	-56.16	-0.01	-55.17	0.00	-55.17	-0.99
	THR 173	3.72	-10.80	-3.54	-10.63	5.19	-10.69	-4.75	-10.26	-0.37
	TYR 210	-0.96	-5.72	0.00	-6.69	-0.25	-5.06	0.00	-5.30	-1.38
	PRO 199	-1.08	-2.70	0.00	-3.77	-0.45	-2.77	0.00	-3.23	-0.55
	HSE 166	-0.01	-2.21	0.00	-2.22	-0.01	-2.10	0.00	-2.11	-0.12
	GLY 205	-0.32	0.09	0.00	-0.23	-0.12	-1.83	0.00	-1.95	1.72
	ILE 216	0.51	-0.44	0.00	0.07	-0.22	0.36	0.00	0.14	-0.07
	TYR 206	-0.82	1.99	0.00	1.18	-0.69	3.14	0.00	2.45	-1.28
	SER 219	-0.10	2.54	0.00	2.44	-0.30	2.83	0.00	2.53	-0.08
	GLY 204	-0.30	2.82	0.00	2.52	-0.14	3.05	0.00	2.91	-0.39
	VAL 174	-0.15	3.01	0.00	2.86	-1.07	4.05	0.00	2.98	-0.12
	VAL 208	-1.09	5.42	-0.55	3.78	20.87	-0.03	0.00	20.85	-17.07
	GLU 159	0.00	43.02	0.00	43.02	0.00	42.22	0.00	42.22	0.80
	ASP 200	-0.29	88.12	0.00	87.83	-0.18	89.15	0.00	88.97	-1.14
	ASP 218	-2.17	129.70	0.00	127.53	-1.74	120.80	0.00	119.06	8.47

Figure S15 – Per-residue energetic contributions in the FGF2-FGFR1/heparin-A predicted (left) and crystal (right) structures for chain D. [PDB: 1FQ9, res. 3.00 Å, RMSD: 1.51/0.75 Å]. See also: Figure 2, S5-S8, S10, S13, S14, S16, and S17.

		Docked				Crystal				
	Residue	**VdW**	**Coulomb**	**H Bond**	**NonBond**	**VdW**	**Coulomb**	**H Bond**	**NonBond**	$\Delta_{NonBond}$
Chain C	ARG 209	1.18	-211.75	-4.98	-215.55	-5.88	-198.45	-3.76	-208.09	-7.46
	LYS 207	12.57	-210.11	-9.85	-207.39	38.55	-204.68	-1.08	-167.22	-40.17
	LYS 175	7.82	-136.79	-5.80	-134.77	-0.95	-127.70	0.00	-128.65	-6.12
	LYS 177	-0.07	-88.11	0.00	-88.18	-0.06	-87.73	0.00	-87.79	-0.39
	LYS 172	-0.05	-79.78	0.00	-79.83	-0.04	-79.56	0.00	-79.60	-0.23
	LYS 160	-0.01	-76.48	0.00	-76.49	-0.01	-76.64	0.00	-76.65	0.16
	LYS 163	-0.01	-63.13	0.00	-63.14	-0.01	-63.12	0.00	-63.12	-0.02
	TYR 210	1.90	-7.94	-3.75	-9.79	-0.36	-6.01	0.00	-6.37	-3.42
	THR 173	-0.99	-7.60	0.00	-8.59	-0.78	-5.25	0.00	-6.03	-2.56
	VAL 168	-0.01	-1.12	0.00	-1.13	-0.01	-1.10	0.00	-1.11	-0.02
	SER 214	-0.31	0.98	0.00	0.68	-0.25	-1.54	0.00	-1.79	2.47
	HSE 166	-0.01	1.28	0.00	1.28	-0.01	1.35	0.00	1.34	-0.07
	ILE 216	2.12	-0.30	0.00	1.82	51.25	-0.18	0.00	51.07	-49.25
	VAL 174	-0.12	3.36	0.00	3.24	-0.10	3.33	0.00	3.24	0.01
	THR 212	-0.65	4.14	0.00	3.49	-0.55	-1.10	0.00	-1.65	5.14
	VAL 208	-1.18	8.37	0.00	7.19	-0.79	8.04	0.00	7.24	-0.05
	ASP 218	-0.99	148.97	0.00	147.98	-0.74	142.16	0.00	141.42	6.56

Figure S16 – Per-residue energetic contributions in the FGF2-FGFR1/heparin-B predicted (left) and crystal (right) structures for chain C. [PDB: 1FQ9, res. 3.00 Å, RMSD: 1.51/0.75 Å]. See also: Figure 2, S5-S8, S10, S13-S15, and S17.

		Docked				Crystal				
	Residue	VdW	Coulomb	H Bond	NonBond	VdW	Coulomb	H Bond	NonBond	$\Delta_{NonBond}$
Chain D	LYS 177	8.65	-171.98	-6.19	-169.52	0.20	-174.51	-3.33	-177.64	8.12
	LYS 175	1.59	-162.42	-4.93	-165.76	-2.60	-161.79	-0.16	-164.55	-1.22
	LYS 172	-0.28	-159.18	-0.78	-160.24	-1.62	-158.79	-0.63	-161.05	0.80
	LYS 163	6.54	-157.81	-4.80	-156.06	-1.33	-141.73	-0.02	-143.09	-12.98
	LYS 160	-1.22	-138.51	0.00	-139.73	3.52	-146.18	0.00	-142.67	2.94
	LYS 207	-0.03	-75.10	0.00	-75.13	-0.04	-75.73	0.00	-75.77	0.64
	ARG 209	-0.04	-71.55	0.00	-71.58	-0.05	-72.21	0.00	-72.25	0.67
	HSE 166	5.13	-14.03	-4.53	-13.43	-0.83	-6.97	0.00	-7.80	-5.63
	SER 214	-0.07	-5.85	0.00	-5.92	-0.10	-2.00	0.00	-2.09	-3.82
	VAL 174	-0.95	-3.15	0.00	-4.10	-1.09	-3.17	0.00	-4.26	0.17
	ILE 216	-0.31	-3.34	0.00	-3.64	-0.44	-3.31	0.00	-3.75	0.11
	VAL 168	-0.27	-2.77	0.00	-3.03	-0.33	-2.64	0.00	-2.97	-0.06
	VAL 208	-0.01	-0.83	0.00	-0.84	-0.02	-0.93	0.00	-0.94	0.10
	THR 212	-0.10	1.83	0.00	1.74	-0.13	0.41	0.00	0.28	1.46
	TYR 210	-0.01	1.78	0.00	1.77	-0.01	2.20	0.00	2.19	-0.41
	THR 173	-1.69	7.34	0.00	5.65	-1.89	3.99	0.00	2.10	3.56
	ASP 218	-0.06	83.76	0.00	83.70	-0.07	83.74	0.00	83.68	0.02

Figure S17 – Per-residue energetic contributions in the FGF2-FGFR1/heparin-B predicted (left) and crystal (right) structures for chain D. [PDB: 1FQ9, res. 3.00 Å, RMSD: 1.51/0.75 Å]. See also: Figure 2, S5-S8, S10, and S13-S16.

		Docked				Crystal				
	Residue	VdW	Coulomb	H Bond	NonBond	VdW	Coulomb	H Bond	NonBond	$\Delta_{NonBond}$
Chain I	ARG 47	5.37	-206.85	-10.73	-212.21	5.88	-194.99	-4.73	-193.85	-18.36
	LYS 114	12.38	-211.46	-10.33	-209.40	-5.92	-219.34	-6.42	-231.68	22.28
	LYS 11	3.13	-202.41	-7.42	-206.70	-6.64	-175.36	0.00	-182.00	-24.70
	ARG 46	9.21	-187.90	-8.44	-187.12	0.31	-171.42	-1.86	-172.98	-14.15
	ARG 13	9.47	-177.67	-12.91	-181.11	-0.70	-117.01	-1.69	-119.39	-61.71
	LYS 125	-1.21	-134.22	0.00	-135.43	176.01	-192.82	-0.26	-17.07	-118.36
	ARG 129	4.95	-129.62	-8.03	-132.71	-0.61	-120.34	-2.08	-123.03	-9.68
	ARG 24	-0.29	-95.38	0.00	-95.67	-0.16	-99.79	0.00	-99.95	4.29
	ARG 132	-0.15	-93.62	0.00	-93.77	-0.36	-100.85	0.00	-101.21	7.44
	ASN 45	-2.51	-17.11	-5.46	-25.08	-4.27	-15.33	-4.67	-24.27	-0.81
	SER 112	-1.18	-11.59	0.00	-12.77	-1.47	1.62	0.00	0.16	-12.93
	PRO 12	-1.66	-8.21	0.00	-9.87	3.69	-10.49	0.00	-6.80	-3.07
	THR 44	-4.47	-3.49	0.00	-7.96	-2.79	0.12	0.00	-2.67	-5.29
	ALA 43	-3.12	-4.65	0.00	-7.77	-3.92	-1.74	0.00	-5.66	-2.12
	VAL 48	-1.15	-5.49	0.00	-6.64	0.26	-6.05	0.00	-5.79	-0.86
	PHE 122	-1.04	-1.68	0.00	-2.72	0.26	-1.98	0.00	-1.71	-1.01
	ILE 40	-0.40	-1.93	0.00	-2.33	-0.29	-2.29	0.00	-2.57	0.25
	PHE 121	-0.37	-1.23	0.00	-1.60	-0.72	-1.42	0.00	-2.14	0.54
	LEU 126	-0.17	-0.39	0.00	-0.56	-0.31	0.04	0.00	-0.27	-0.29
	LEU 417	-0.20	-0.32	0.00	-0.53	-0.24	-0.48	0.00	-0.72	0.20
	GLN 118	-0.23	0.24	0.00	0.01	-0.50	-4.03	0.00	-4.53	4.55
	THR 115	-0.42	0.54	0.00	0.12	-0.42	3.03	0.00	2.61	-2.49
	PRO 41	-0.26	5.91	0.00	5.65	-0.17	4.70	0.00	4.53	1.12
	GLU 42	-0.54	79.06	0.00	78.53	-0.39	89.43	0.00	89.04	-10.51
	GLU 113	1.90	92.68	-1.04	93.55	11.78	97.20	0.00	108.98	-15.43
	ASP 14	-0.11	107.49	0.00	107.38	-0.30	116.97	0.00	116.66	-9.29

Figure S18 – Per-residue energetic contributions in the Antithrombin-III/heparin analog predicted (left) and crystal (right) structures. [PDB: 1E03, res. 2.90 Å, RMSD: 0.60 Å]. See also: Figure 2, S9, and S10.

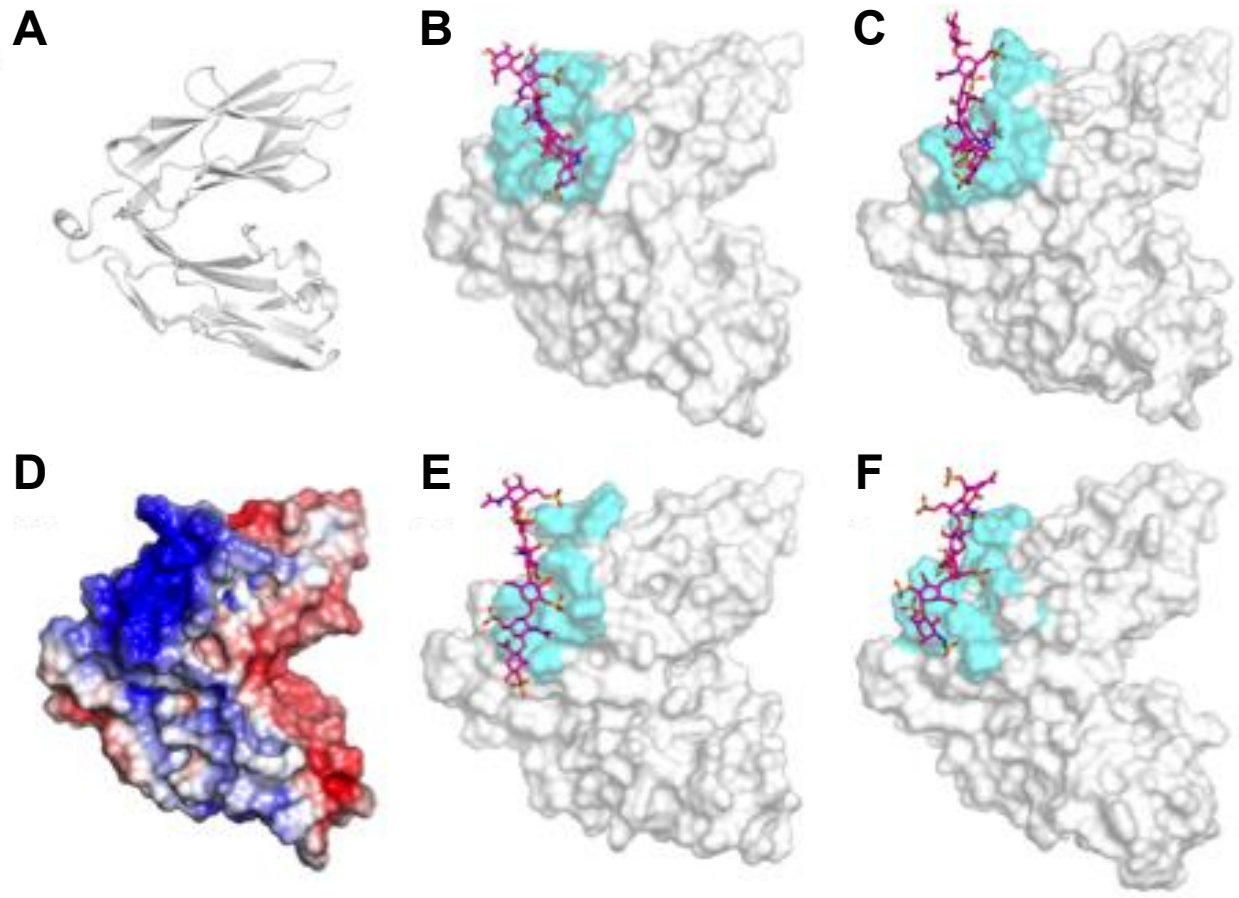

Figure S19 – RPTPσ. (A) Ig1 and Ig2 domains of RPTPσ. (D) Electrostatic potential surface. (B, C, E, F) Predicted structures of CS-A, CS-D, CS-E, and heparin after docking and molecular dynamics. See also: Figure 3, S20-S23, S37, and S38.

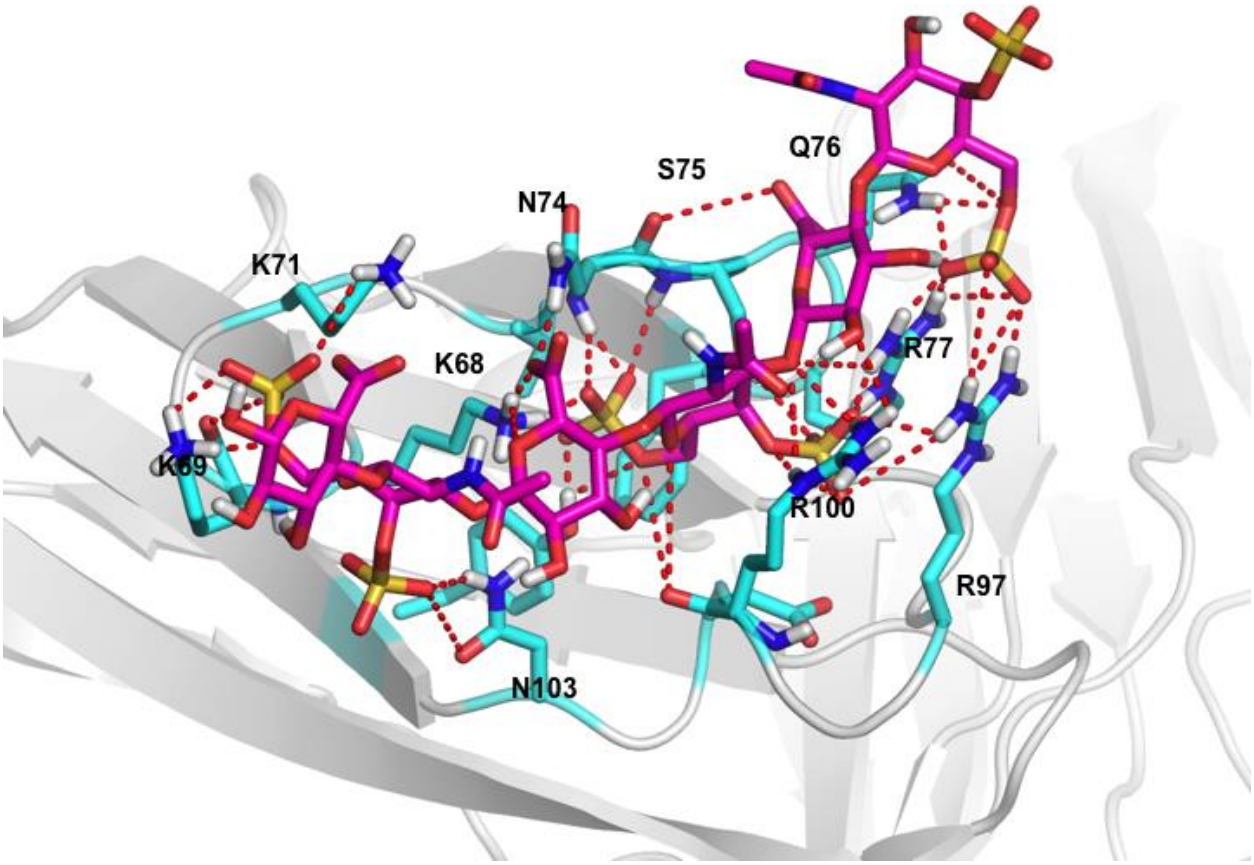

Figure S20 – Predicted structure of CS-E hexamer (magenta) bound to RPTPσ with 5 Å binding site shown (cyan). Dashed lines indicate hydrogen bonding and salt bridges between ligand and protein. See also: Figure 3, S19, S21-S23, S37, and S38.

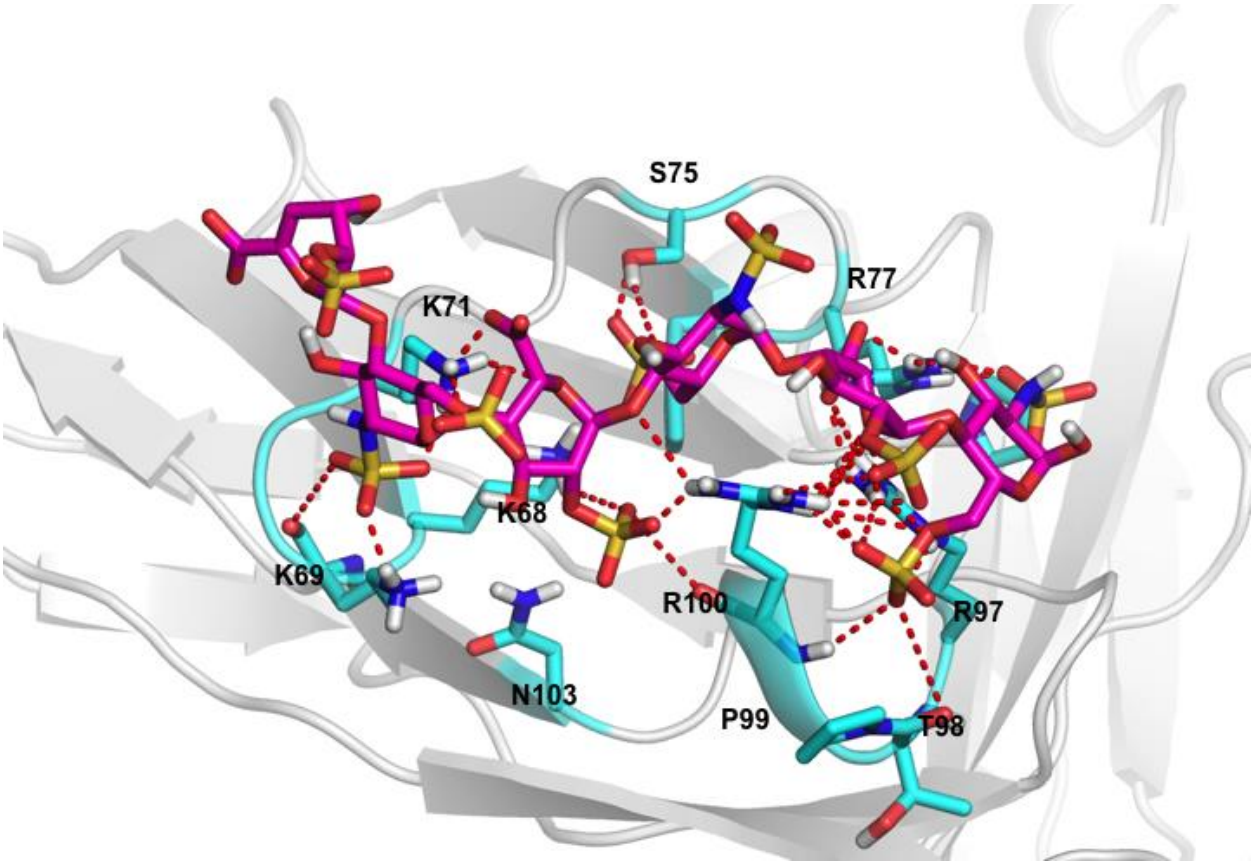

Figure S21 – Predicted structure of heparin hexamer (magenta) bound to RPTPσ with 5 Å binding site shown (cyan). Dashed lines indicate hydrogen bonding and salt bridges between ligand and protein. See also: Figure 3, S19-S20, S22-S23, S37, and S38.

	CS-A				CS-D			
Residue	**VdW**	**Coulomb**	**H Bond**	**NonBond**	**VdW**	**Coulomb**	**H Bond**	**NonBond**
ARG 76	2.59	-109.82	-8.26	-115.50	2.85	-152.95	-10.80	-160.91
LYS 67	9.11	-108.48	-12.32	-111.69	-0.54	-100.52	0.00	-101.06
ARG 99	-2.41	-90.30	-2.04	-94.75	11.00	-174.16	25.17	-188.33
ARG 96	9.71	-89.82	-11.85	-91.97	-0.68	-134.41	-4.42	-139.50
LYS 71	-1.67	-85.86	0.00	-87.54	14.26	-141.64	-11.80	-139.20
LYS 68	2.01	-99.90	-6.62	-104.51	-0.19	-76.14	0.00	-76.33
LYS 71	--	--	--	--	-0.46	-75.57	0.00	-76.03
GLN 75	-1.67	-7.74	-4.48	-13.89	1.86	-16.06	-8.45	-22.65
ASN 73	-0.86	2.13	0.00	1.27	-0.30	-0.29	-5.86	-6.45
SER 74	4.90	-12.36	-4.75	-12.21	-2.31	-6.93	0.00	-9.24
ASN 102	-1.20	-2.24	0.00	-3.44	-0.15	-10.6	0.00	-1.20
GLU 101	-0.23	48.03	0.00	47.80	--	--	--	--
GLY 69	--	--	--	--	--	--	--	--
PRO 94	--	--	--	--	-1.05	1.32	0.00	0.27
PRO 98	--	--	--	--	--	--	--	--
THR 97	--	--	--	--	-0.19	1.83	0.00	1.65
VAL 73	-0.82	-2.94	0.00	-3.77	-0.30	-1.35	0.00	-1.65
TYR 104	--	--			-0.09	-2.46	0.00	-2.55
PHE 77	-3.66	-1.37	0.00	-5.03	--	--	--	--
ASP 100	-0.63	75.50	0.00	74.88	--	--	--	--

Figure S22 – Per-residue energetic contributions in the predicted RPTPσ/CS-A (left) and RPTPσ/CS-D (right) structures. See also: Figure 3, S19-S21, S23, S37, and S38.

	CS-E				Heparin			
Residue	**VdW**	**Coulomb**	**H Bond**	**NonBond**	**VdW**	**Coulomb**	**H Bond**	**NonBond**
ARG 76	11.74	-158.46	-17.21	-163.92	0.89	-180.82	-7.26	-187.18
LYS 67	10.98	-158.86	-10.24	-158.12	-0.60	-170.34	-1.68	-172.61
ARG 99	-0.66	-139.54	-9.43	-149.63	3.44	-208.70	-9.97	-215.23
ARG 96	1.84	-137.33	-5.15	-140.64	2.01	-180.78	-8.27	-187.04
LYS 71	-2.11	-131.74	0.00	-133.86	4.10	-223.34	-3.40	-222.65
LYS 68	3.46	-115.00	-5.67	-117.21	-1.69	-127.16	0.00	-128.85
LYS 71	-0.37	-65.91	0.00	-66.28	--	--	--	--
GLN 75	5.83	-20.07	-12.97	-27.22	-0.17	-5.26	0.00	-5.43
ASN 73	2.57	-15.72	-10.33	-23.48	-0.22	-1.46	0.00	-1.68
SER 74	-1.95	-10.28	-0.59	-12.83	-0.85	-7.68	-0.18	-8.71
ASN 102	-1.49	-9.18	0.00	-10.67	-0.26	-9.19	0.00	-9.45
GLU 101	--	--	--	--	--	--	--	--
GLY 69	--	--	--	--	-0.15	0.74	0.00	0.59
PRO 94	--	--	--	--	-0.54	4.62	0.00	4.08
PRO 98	--	--	--	--	-1.04	-2.44	0.00	-3.47
THR 97	--	--	--	--	-0.28	3.73	0.00	3.45
VAL 73	-2.38	-5.93	0.00	-8.31	--	--	--	--
TYR 104	3.55	-6.81	-4.76	-8.02	--	--	--	--
PHE 77	-3.37	1.18	0.00	-2.19	-1.31	-0.46	0.00	-1.77
ASP 100	-1.75	97.79	0.00	96.04	--	--	--	--

Figure S23 – Per-residue energetic contributions in the predicted RPTPσ/CS-E (left) and RPTPσ/heparin (right) structures. See also: Figure 3, S19-S22, S37, and S38.

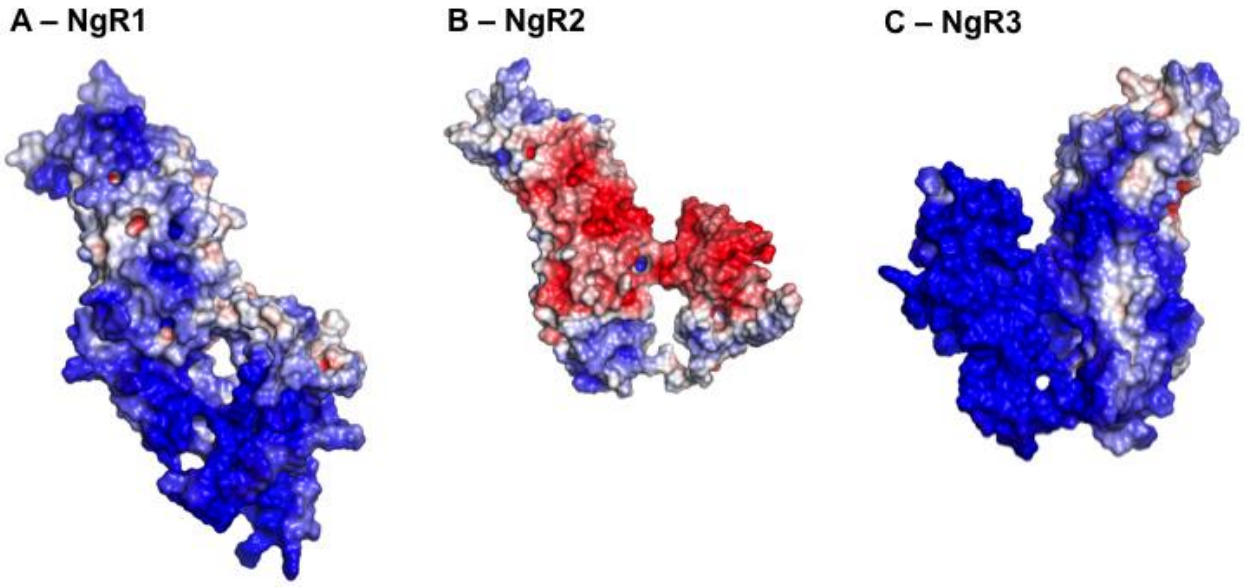

Figure S24 – Electrostatic potential surfaces of (A) NgR1, (B) NgR2, and (C) NgR3. Note the lack of positive charge on NgR2, but strong positive charge on NgR1 and NgR3. See also: Figure 4, and S25-S36 and S39-S42.

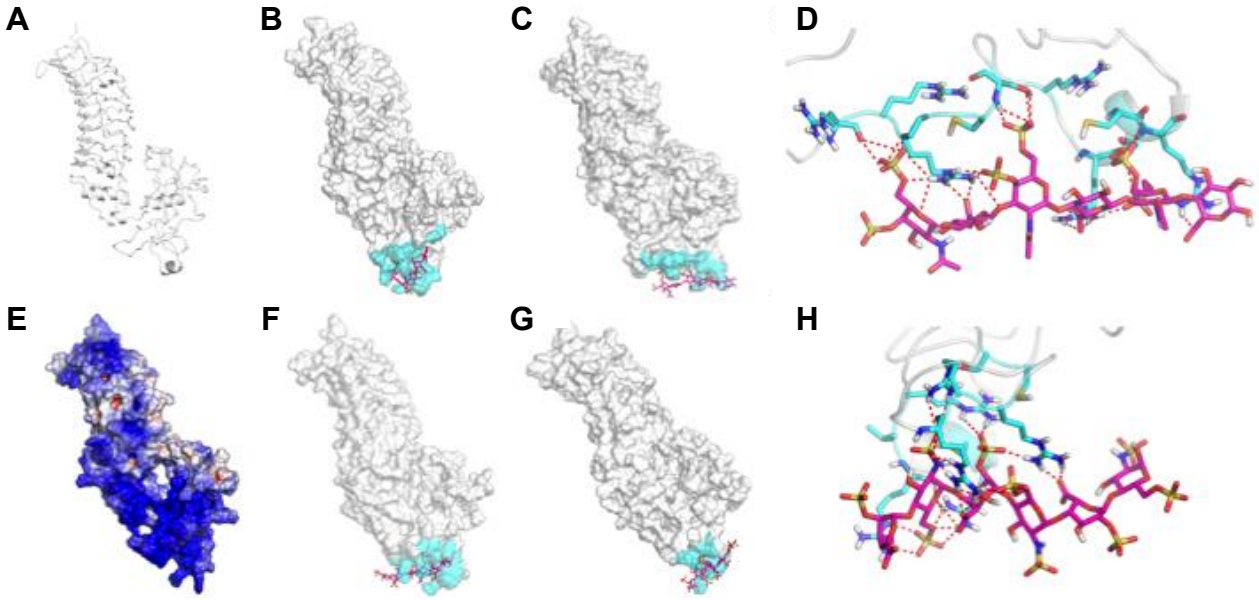

Figure S25 – NgR1. (A) Structure of NgR1. (E) Electrostatic potential surface showing strong positive charge. (B, C, F, G) Predicted structures of CS-A, CS-D, CS-E, and heparin after docking and molecular dynamics. (D, H) Detailed view of CS-E and heparin predicted structures. See also: Figure 4, S24, S26-S31, S39, and S40.

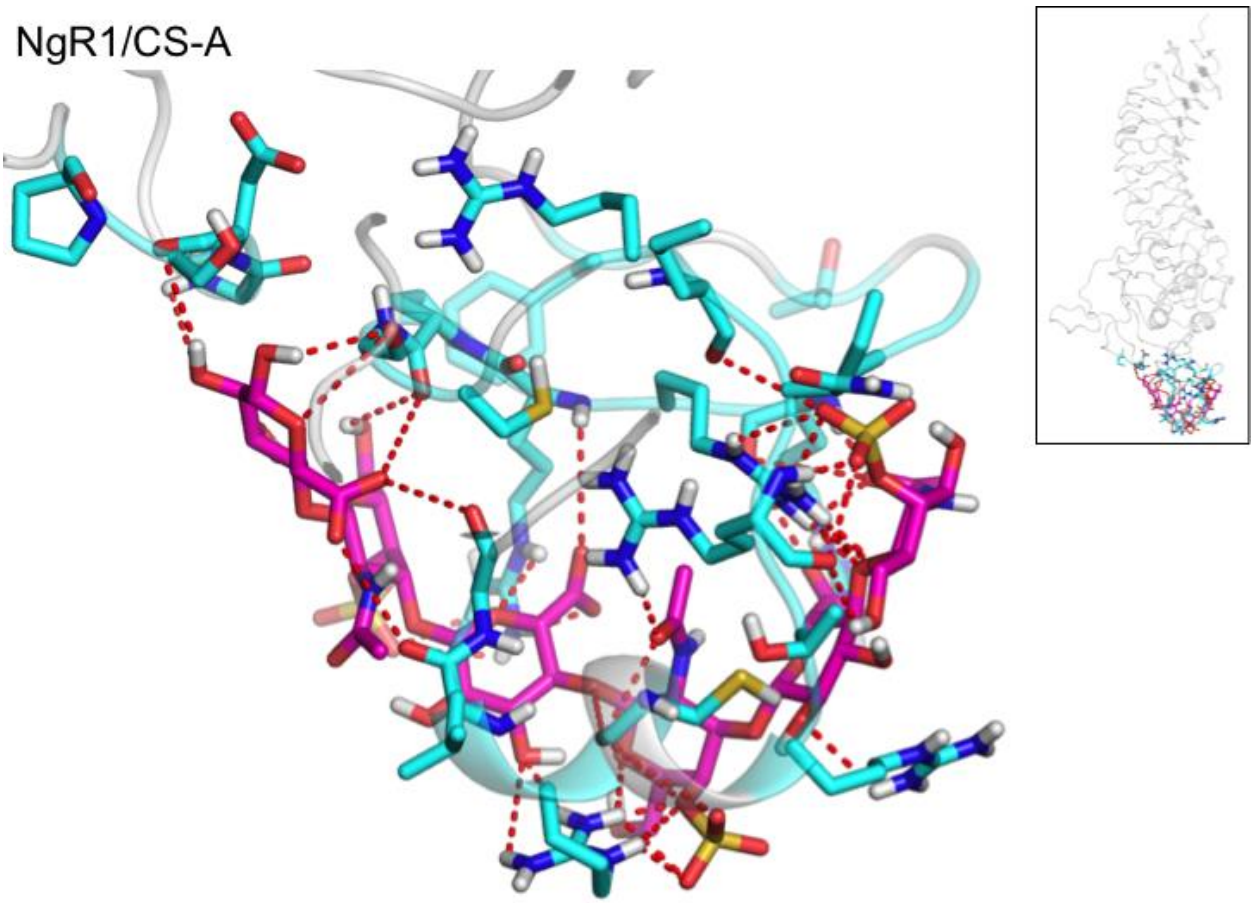

Figure S26 – Detail of predicted NgR1/CS-A structure after docking and dynamics with CS-A hexamer (magenta) and 5 Å binding site (cyan) shown. Dashed lines indicate hydrogen bonding and salt bridges between ligand and protein. Overall placement on protein shown in inset. See also: Figure 4, S24-S25, S27-S31, S39, and S40.

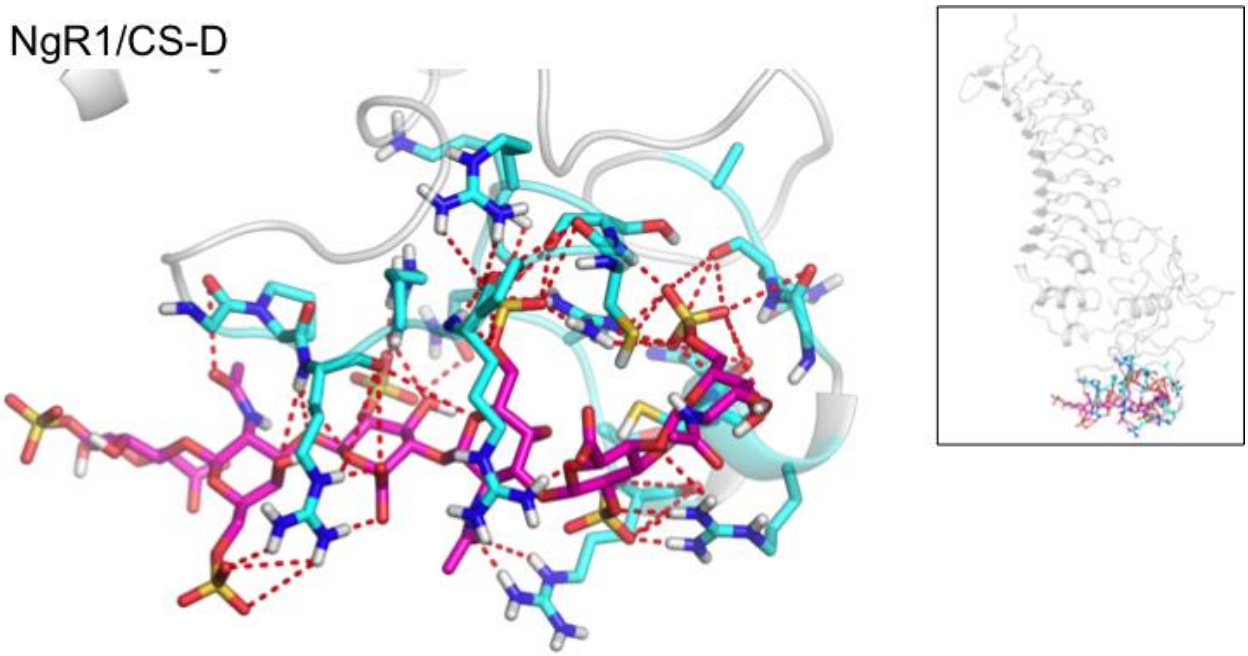

Figure S27 – Detail of predicted NgR1/CS-D structure after docking and dynamics with CS-D hexamer (magenta) and 5 Å binding site (cyan) shown. Dashed lines indicate hydrogen bonding and salt bridges between ligand and protein. Overall placement on protein shown in inset. See also: Figure 4, S24-26, S27-S31, S39, and S40.

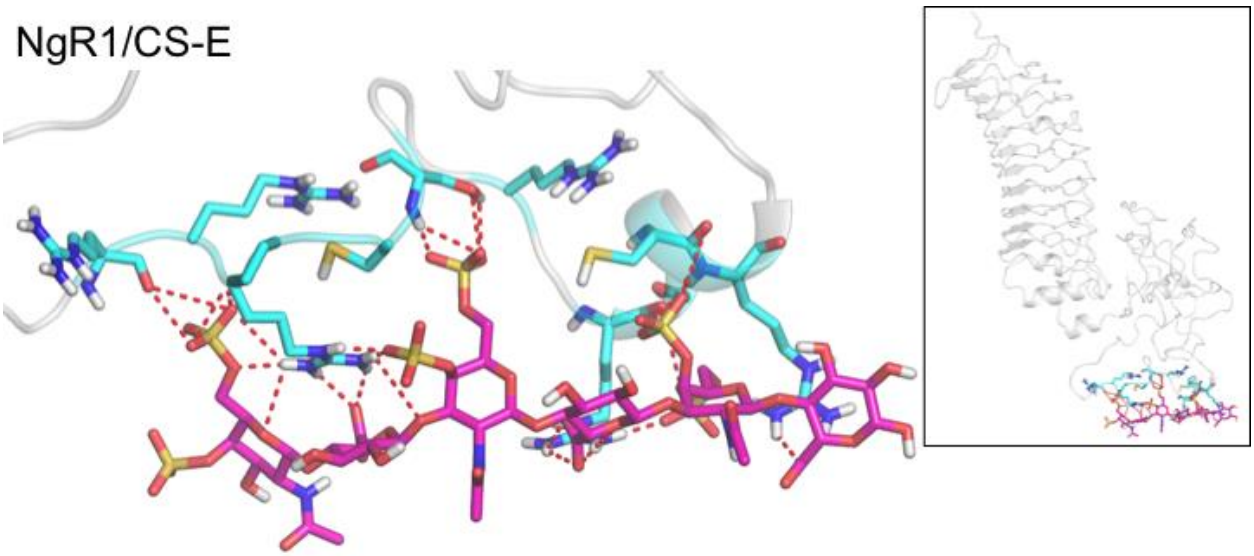

Figure S28 – Detail of predicted NgR1/CS-E structure after docking and dynamics with CS-E hexamer (magenta) and 5 Å binding site (cyan) shown. Dashed lines indicate hydrogen bonding and salt bridges between ligand and protein. Overall placement on protein shown in inset. See also: Figure 4, S24-S27, S29-S31, S39, and S40.

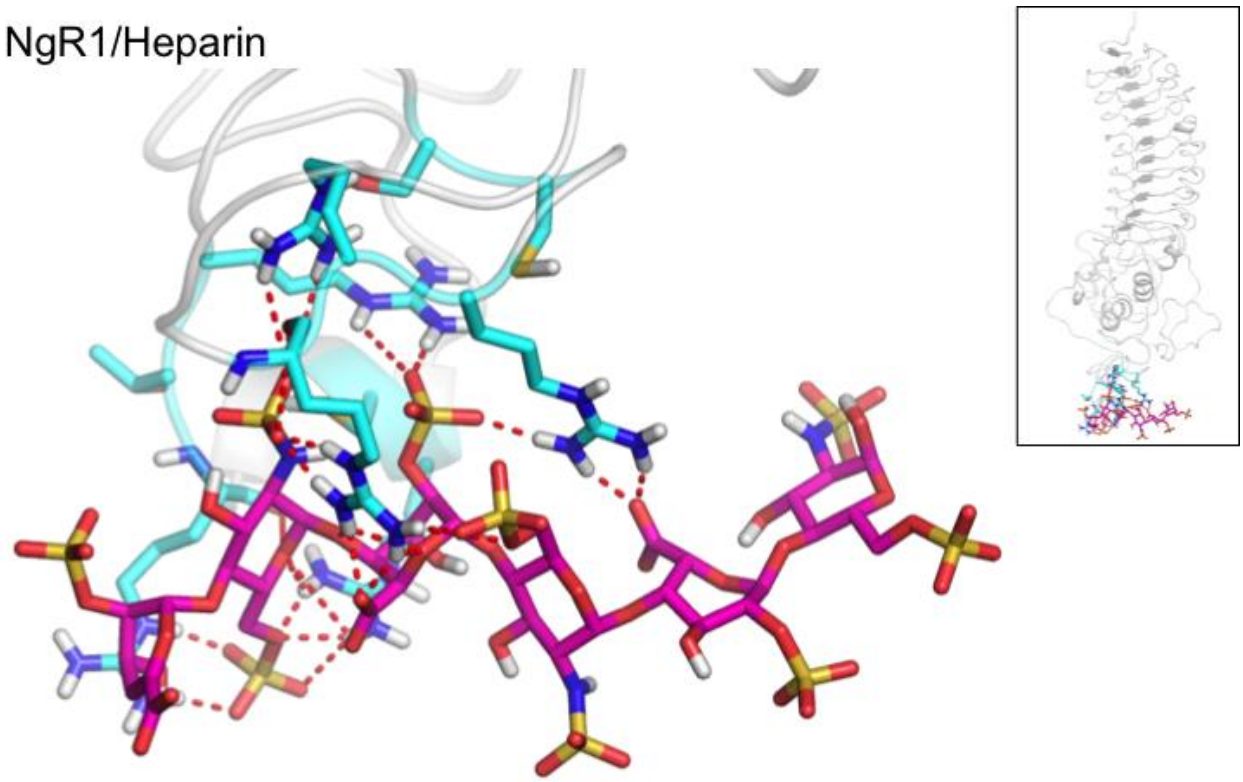

Figure S29 – Detail of predicted NgR1/heparin structure after docking and dynamics with heparin hexamer (magenta) and 5 Å binding site (cyan) shown. Dashed lines indicate hydrogen bonding and salt bridges between ligand and protein. Overall placement on protein shown in inset. See also: Figure 4, S24-S28, S30-S31, S39, and S40.

		CS-A				CS-D				CS-E				Heparin			
Residue		VdW	Coulomb	H Bond	NonBond	VdW	Coulomb	H Bond	NonBond	VdW	Coulomb	H Bond	NonBond	VdW	Coulomb	H Bond	NonBond
ARG	390	6.94	-90.88	-13.23	-97.17	2.15	-136.95	-11.48	-146.28	-1.11	-61.48	0.00	-62.59	5.12	-213.83	-16.07	-224.78
ARG	392	-2.73	-107.51	-5.79	-116.04	-2.26	-126.71	-8.96	-137.93	-0.19	-158.71	-14.92	-173.82	2.77	-191.60	-10.23	-199.06
ARG	406	-2.67	-96.20	-7.45	-106.33	4.79	-116.69	-8.19	-120.09	2.55	-131.51	-12.53	-141.50	-1.21	-176.87	-6.87	-184.95
ARG	402	-3.57	-69.97	0.00	-73.53	0.76	-120.34	-4.53	-124.10	3.02	-147.77	-12.85	-157.59	0.82	-151.54	-9.09	-159.81
ARG	400	-0.48	-96.72	-5.19	-102.39	8.97	-144.72	-15.76	-151.51	-0.73	-98.90	0.00	-99.63	4.04	-142.10	-5.53	-143.59
ARG	391	-2.06	-111.17	-8.33	-121.56	1.17	-142.38	-7.89	-149.09	-1.38	-105.45	0.00	-106.83	-1.06	-134.39	0.00	-135.44
ARG	397	-0.25	-56.79	0.00	-57.04	-1.74	-101.89	-0.03	-103.66	-0.15	-72.85	0.00	-73.00	-0.06	-96.30	0.00	-96.36
LYS	398	-0.40	-40.49	0.00	-40.89	-0.78	-81.71	0.00	-82.49	-0.14	-58.40	0.00	-58.54	-0.06	-68.64	0.00	-68.70
PRO	389	-4.08	-5.91	0.00	-9.99	-4.13	-4.22	0.00	-8.34	-0.33	-3.98	0.00	-4.31	-0.36	-4.12	0.00	-4.48
GLY	408	-1.82	-0.24	0.00	-2.06	-0.81	-5.51	0.00	-6.32	-0.09	-4.24	0.00	-4.33	-0.07	-4.17	0.00	-4.24
GLY	388	-0.62	-3.62	0.00	-4.24	-0.96	-6.68	0.00	-7.64	-0.04	-3.15	0.00	-3.19	-0.03	-4.10	0.00	-4.13
CYS	405	-1.71	0.31	-2.35	-3.75	-0.20	-5.66	-2.02	-7.88	-0.01	-8.79	0.00	-8.80	-3.89	-0.16	0.00	-4.05
ASN	399	-1.35	-5.54	0.00	-6.89	-1.93	1.27	0.00	-0.65	-0.19	-4.50	0.00	-4.70	-0.31	-3.64	0.00	-3.95
PHE	384	-0.69	-1.25	0.00	-1.94	-0.23	-2.07	0.00	-2.30	-0.03	-1.51	0.00	-1.55	-0.07	-2.90	0.00	-2.97
LEU	407	-0.98	0.71	0.00	-0.27	-0.25	-1.87	0.00	-2.12	-0.27	-1.86	0.00	-2.14	-0.07	-1.97	0.00	-2.04
GLY	394	1.03	-2.84	0.00	-1.81	-0.56	0.65	0.00	0.09	-0.50	0.68	0.00	0.18	-0.05	-1.33	0.00	-1.38
CYS	395	-2.02	-1.44	0.00	-3.46	-0.43	-9.15	0.00	-9.58	-2.79	-12.58	0.00	-15.37	-0.65	-0.26	0.00	-0.91
SER	344	-0.83	-0.23	0.00	-1.07	-0.11	-0.55	0.00	-0.66	-0.01	-1.48	0.00	-1.49	-0.02	-0.19	0.00	-0.21
THR	444	0.00	-0.53	0.00	-0.53	-0.01	1.78	0.00	1.78	0.00	-0.46	0.00	-0.46	0.00	0.64	0.00	0.64
ALA	410	-0.17	-0.76	0.00	-0.93	-0.24	0.61	0.00	0.37	-0.02	-0.05	0.00	-0.07	-0.03	1.06	0.00	1.03
THR	386	-0.20	0.59	0.00	0.39	-0.06	1.06	0.00	1.00	-0.01	1.22	0.00	1.21	-0.01	1.16	0.00	1.15
HSE	404	-0.48	1.27	0.00	0.79	-0.60	2.33	0.00	1.73	-0.29	0.25	0.00	-0.04	-0.23	1.87	0.00	1.63
GLN	409	-0.49	1.79	0.00	1.30	-1.17	9.18	0.00	8.01	-0.07	3.92	0.00	3.85	-0.07	2.02	0.00	1.95
PRO	345	-0.13	0.77	0.00	0.64	-0.04	1.85	0.00	1.82	0.00	1.29	0.00	1.29	-0.01	2.08	0.00	2.08
GLY	342	-0.99	-1.11	0.00	-2.10	-0.04	2.58	0.00	2.55	-0.01	1.93	0.00	1.93	-0.02	2.20	0.00	2.18
THR	401	-0.66	2.74	0.00	2.08	-0.46	4.98	0.00	4.52	-0.37	3.92	0.00	3.55	-0.72	3.17	0.00	2.45
SER	396	-0.18	3.43	0.00	3.25	0.59	5.47	-3.85	2.21	3.30	-2.21	-4.89	-3.80	-0.18	2.69	0.00	2.51
PRO	393	-3.03	4.64	0.00	1.61	-0.79	7.05	0.00	6.26	-0.40	7.33	0.00	6.92	-0.24	5.85	0.00	5.61
SER	403	-0.18	3.43	0.00	3.25	-0.19	2.81	0.00	2.61	-1.02	1.80	0.00	0.78	-0.35	6.34	0.00	5.99
ASP	343	-1.62	48.13	0.00	46.51	-0.07	71.82	0.00	71.74	-0.01	61.99	0.00	61.98	-0.02	82.58	0.00	82.56

Figure S30 – Per-residue energetic contributions in the predicted NgR1 structures for CS-A, CS-D, CS-E, and heparin. See also: Figure 4, S24-S29, S31, S39, and S40.

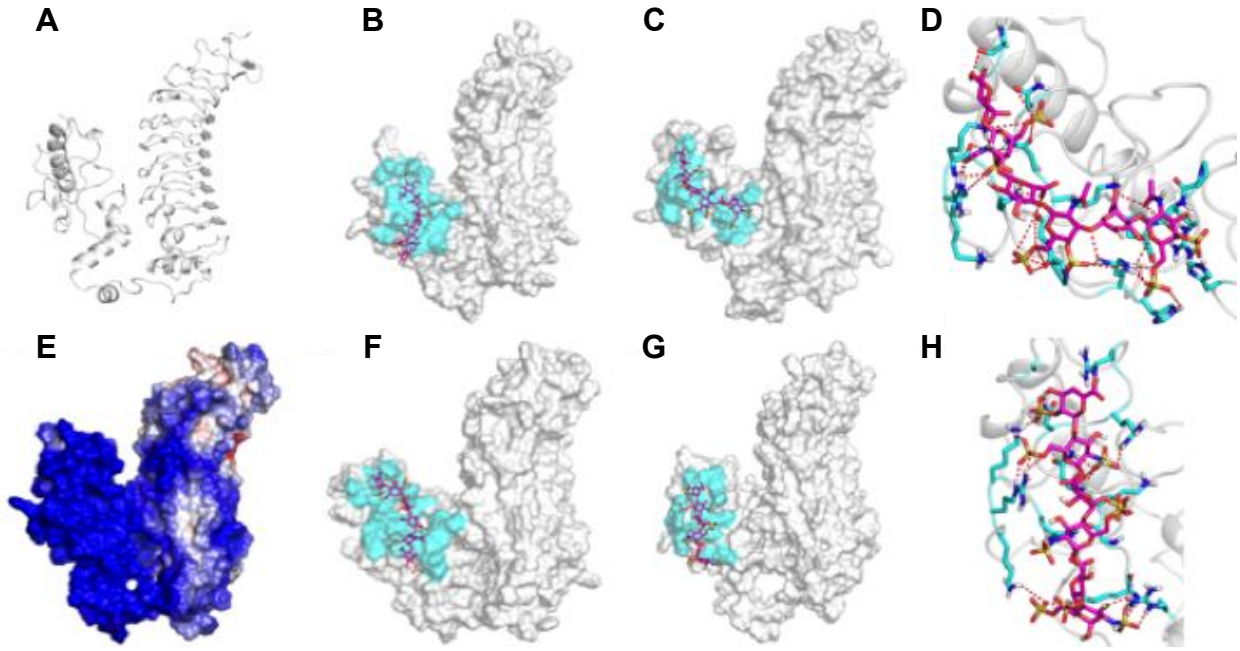

Figure S31 – NgR3. (A) Structure of NgR3. (E) Electrostatic potential surface. (B, C, F, G) Predicted structures of CS-A, CS-D, CS-E, and heparin after docking and molecular dynamics. (D, H) Detailed view of CS-E and heparin predicted structures. See also: Figure 4, S24, and S32-S36, S41, and S42.

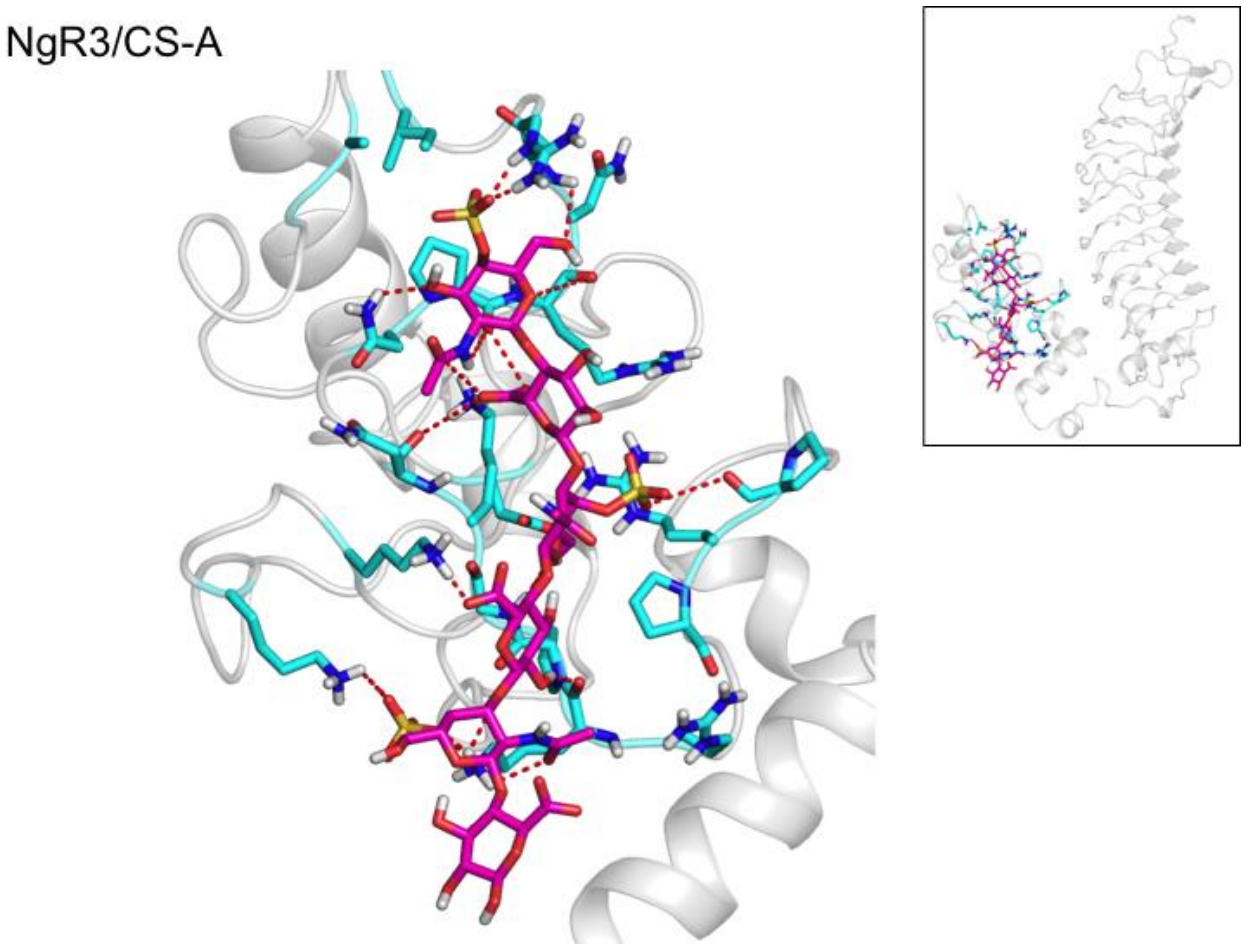

Figure S32 – Detail of predicted NgR3/CS-A structure after docking and dynamics with CS-A hexamer (magenta) and 5 Å binding site (cyan) shown. Dashed lines indicate hydrogen bonding and salt bridges between ligand and protein. Overall placement on protein shown in inset. See also: Figure 4, S24, S31, S33-S36, S41, and S42.

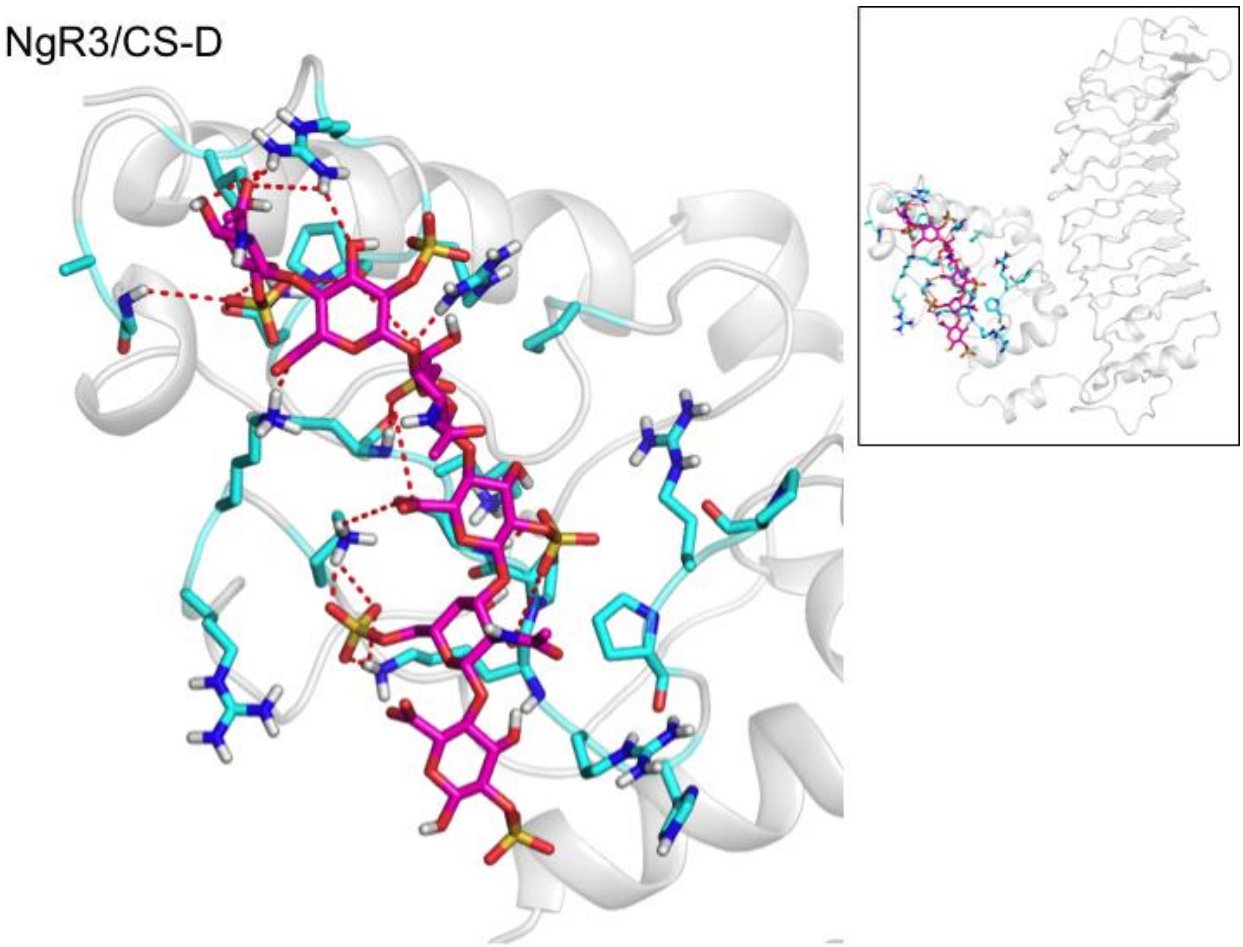

Figure S33 – Detail of predicted NgR3/CS-D structure after docking and dynamics with CS-D hexamer (magenta) and 5 Å binding site (cyan) shown. Dashed lines indicate hydrogen bonding and salt bridges between ligand and protein. Overall placement on protein shown in inset. See also: Figure 4, S24, S31, S32, S34-S36, S41, and S42.

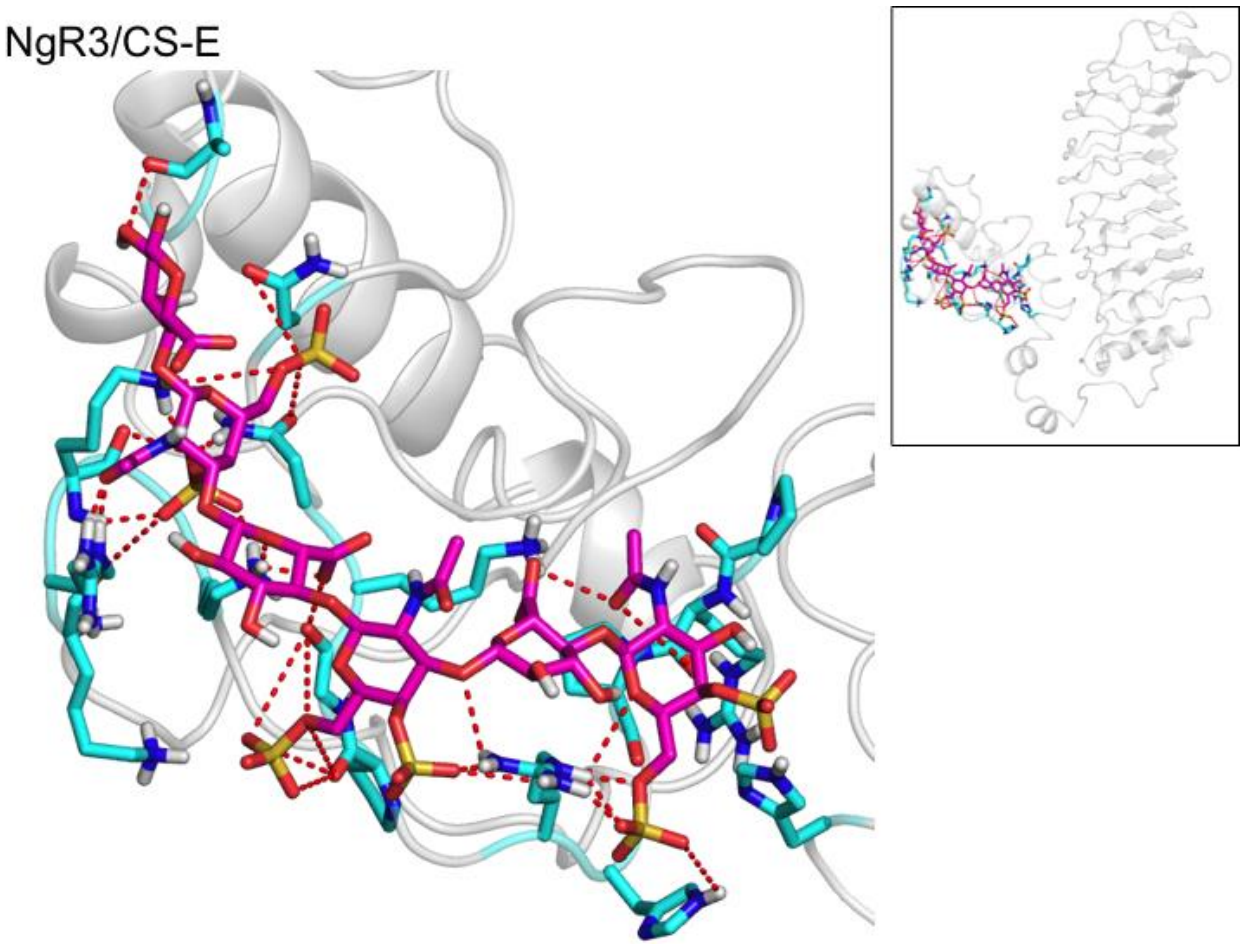

Figure S34 – Detail of predicted NgR3/CS-E structure after docking and dynamics with CS-E hexamer (magenta) and 5 Å binding site (cyan) shown. Dashed lines indicate hydrogen bonding and salt bridges between ligand and protein. Overall placement on protein shown in inset. See also: Figure 4, S24, S31-S33, S35, S36, S41, and S42.

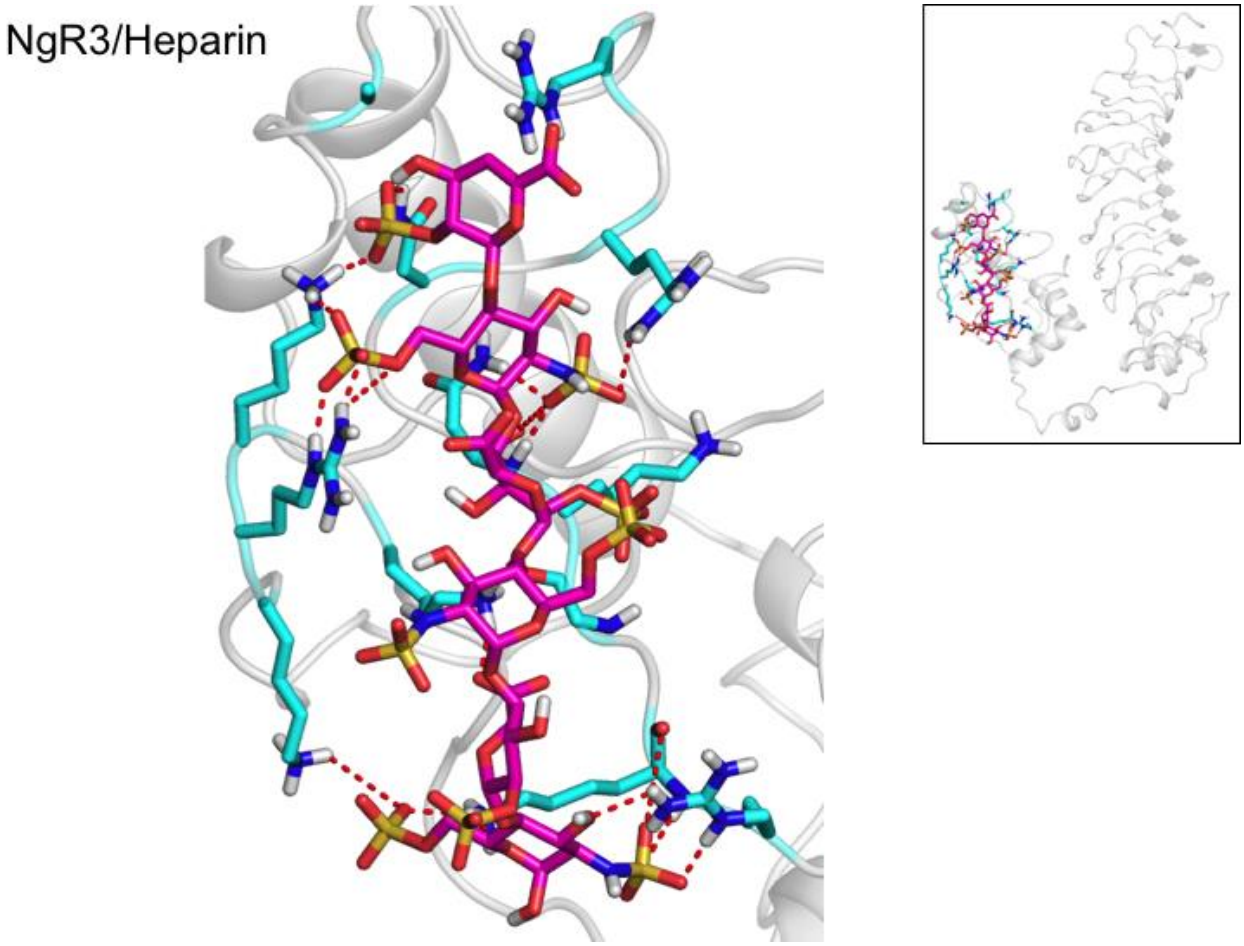

Figure S35 – Detail of predicted NgR3/heparin structure after docking and dynamics with heparin hexamer (magenta) and 5 Å binding site (cyan) shown. Dashed lines indicate hydrogen bonding and salt bridges between ligand and protein. Overall placement on protein shown in inset. See also: Figure 4, S24, S31-S34, S36, S41, and S42.

		CS-A				CS-D				CS-E				Heparin			
Residue		VdW	Coulomb	H Bond	NonBond	VdW	Coulomb	H Bond	NonBond	VdW	Coulomb	H Bond	NonBond	VdW	Coulomb	H Bond	NonBond
LYS	383	4.11	-102.12	-2.70	-100.71	0.45	-152.91	-4.15	-156.61	6.52	-162.33	-9.44	-165.24	7.58	-206.62	-11.23	-210.27
ARG	380	-0.04	-40.12	0.00	-40.16	-1.06	-102.20	0.00	-103.26	-1.20	-119.85	-5.80	-126.85	3.48	-182.45	-7.59	-186.56
LYS	381	-0.17	-52.67	0.00	-52.84	0.75	-138.39	-4.12	-141.76	4.02	-139.02	-10.71	-145.71	7.81	-180.38	-6.68	-179.25
ARG	330	-0.84	-63.93	0.00	-64.77	-2.80	-102.67	0.00	-105.47	-0.31	-153.39	-11.01	-164.70	2.79	-158.26	-5.44	-160.90
ARG	340	-2.65	-68.57	0.00	-71.22	1.84	-118.19	-5.24	-121.59	-0.29	-83.03	0.00	-83.32	-1.34	-156.72	-2.65	-160.71
LYS	331	-0.27	-98.70	-4.75	-103.72	3.13	-123.36	-5.79	-126.02	-0.63	-74.84	0.00	-75.48	-0.71	-153.93	-0.76	-155.40
LYS	334	-1.13	-89.69	-4.68	-95.50	-2.39	-97.83	0.00	-100.22	-2.53	-141.48	-1.46	-145.47	-3.30	-134.35	0.00	-137.65
LYS	379	-0.84	-81.40	-0.02	-82.25	-0.17	-67.58	0.00	-67.74	-0.37	-84.61	0.00	-84.99	-1.05	-130.60	0.00	-131.66
ARG	342	2.01	-72.80	-6.37	-77.17	-2.08	-104.32	-3.28	-109.68	-0.09	-68.84	0.00	-68.93	-0.81	-118.99	0.00	-119.80
ARG	326	-1.18	-62.89	0.00	-64.07	-0.84	-92.99	0.00	-93.83	-2.41	-72.84	0.00	-75.25	-0.08	-97.25	0.00	-97.33
ASN	335	-1.84	0.07	0.00	-1.77	2.32	-9.47	-4.60	-11.75	-1.99	-9.78	-3.64	-15.41	-0.19	-12.30	-6.78	-19.27
ASN	338	-1.39	-2.82	-0.16	-4.37	-1.61	-2.72	-0.08	-4.41	-1.12	-2.24	0.00	-3.37	-1.17	-3.49	0.00	-4.66
PRO	362	-0.25	-0.75	0.00	-1.00	-0.20	-2.05	0.00	-2.25	-0.02	-1.54	0.00	-1.57	-0.02	-2.42	0.00	-2.44
PRO	327	-0.88	-3.14	0.00	-4.01	-0.87	-3.83	0.00	-4.70	-3.57	0.38	0.00	-3.18	-0.22	-1.95	0.00	-2.17
GLY	333	0.34	-0.67	-4.29	-4.63	-1.59	-1.25	-3.92	-6.77	-2.38	4.27	0.00	1.89	-1.51	-0.23	0.00	-1.74
GLY	382	-0.09	0.75	0.00	0.66	-0.12	2.17	0.00	2.05	-1.28	1.34	0.00	0.06	-0.25	-1.36	0.00	-1.61
ILE	345	-0.85	-0.11	0.00	-0.96	-1.88	-0.42	0.00	-2.30	-0.12	-0.55	0.00	-0.67	-0.08	-0.78	0.00	-0.86
ALA	350	-0.30	-2.38	0.00	-2.68	-0.12	-1.27	0.00	-1.39	-0.13	-0.71	0.00	-0.84	-0.02	-0.79	0.00	-0.81
ASN	341	-1.36	0.73	0.00	-0.63	-0.15	2.42	0.00	2.27	-0.04	0.79	0.00	0.75	-0.06	0.00	0.00	-0.07
GLY	349	-0.16	-2.75	0.00	-2.91	-0.45	-4.02	0.00	-4.47	-1.21	-2.14	0.00	-3.35	-0.06	0.43	0.00	0.37
PRO	332	-2.68	-0.11	0.00	-2.79	-1.95	-2.37	0.00	-4.32	-0.92	4.48	0.00	3.55	-0.59	1.27	0.00	0.68
PRO	339	-4.19	5.10	0.00	0.92	-0.55	8.20	0.00	7.65	-0.28	5.86	0.00	5.59	-0.26	1.69	0.00	1.43
ALA	348	-0.46	-3.28	0.00	-3.74	-0.29	-2.64	0.00	-2.93	-1.34	-2.64	0.00	-3.97	-0.44	2.12	0.00	1.69
HSE	309	-0.02	-0.37	0.00	-0.40	-0.02	0.60	0.00	0.58	-0.65	-1.57	0.00	-2.21	-0.02	1.89	0.00	1.87
HSE	329	-0.06	0.65	0.00	0.58	-0.27	0.00	0.00	-0.26	-1.25	-1.38	0.00	-2.63	-0.26	3.43	0.00	3.18
PRO	325	-0.44	3.13	0.00	2.69	-0.19	3.21	0.00	3.03	-2.53	-1.17	0.00	-3.70	-0.03	3.36	0.00	3.33
ASP	359	-0.30	64.07	0.00	63.78	-0.04	79.36	0.00	79.32	-0.03	69.11	0.00	69.09	-0.08	100.87	0.00	100.79

Figure S36 – Per-residue energetic contributions in the predicted NgR3 structures for CS-A, CS-D, CS-E, and heparin. See also: Figure 4, S24, S31-S35, S41, and S42.

PTPS - Increased Binding (Relative Energy)					
Set	CSA	CSD	CSE	HEP	Mutations
G1	-1.7	-0.3	-34.2	30.5	V73N S75N Q76N F78Q
G2	-6.2	-35.0	12.6	29.7	N74Q S75N
G3	-17.8	-23.8	-29.0	21.2	V73Q S75N Q76N F78N N103Q

PTPS - Loss of Binding (Relative Energy)					
Set	CSA	CSD	CSE	HEP	Mutations
L1	565.5	719.2	709.8	1059.6	K68Q K69N K71Q R77N R97N R100N
L2	386.0	528.2	481.5	705.1	K71N R77Q R97N R100Q
L3	383.5	472.6	458.7	657.3	K68N K69Q R77N R100N
L4	468.6	629.7	603.3	891.1	K68N K71Q R77N R97N R100Q

PTPS - Increased Binding (Percent Change)					
Set	CSA	CSD	CSE	HEP	Mutations
G1	0.3	0.0	4.2	-2.9	V73N S75N Q76N F78Q
G2	1.1	4.5	-1.6	-2.8	N74Q S75N
G3	3.1	3.1	3.6	-2.0	V73Q S75N Q76N F78N N103Q

PTPS - Loss of Binding (Percent Change)					
Set	CSA	CSD	CSE	HEP	Mutations
L1	-97.3	-92.8	-87.8	-101.0	K68Q K69N K71Q R77N R97N R100N
L2	-66.4	-68.1	-59.6	-67.2	K71N R77Q R97N R100Q
L3	-66.0	-61.0	-56.7	-62.7	K68N K69Q R77N R100N
L4	-80.6	-81.2	-74.6	-84.9	K68N K71Q R77N R97N R100Q

Figure S37 – Predicted sets of mutations to either increase (left) or decrease (right) binding of ligands to RPTPσ. Note that none of the sets show improved binding for heparin. Changes in binding energy are shown relative to the wild-type structures in both absolute change (kcal/mol) and in terms of percent change.

PTPS Increased Binding																		
PTPS Residue			Per-Res ΔHBond				CSA Cavity			CSD Cavity			CSE Cavity			HEP Cavity		
num	from	to	CSA	CSD	CSE	HEP	ΔCav	Δ(HB+VDW)	ΔCou	ΔCav	Δ(HB+VDW)	ΔCou	ΔCav	Δ(HB+VDW)	ΔCou	ΔCav	Δ(HB+VDW)	ΔCou
73	V	N	-1.48	0.00	-6.17	0.00	1.56	-6.53	8.09	5.03	7.96	-2.93	-28.66	3.08	-31.75	-1.41	-2.47	1.07
73	V	Q	-1.82	0.00	0.00	0.00	-2.36	-5.15	2.78	-3.85	5.70	-9.56	-32.20	-6.47	-25.73	-5.87	-0.20	-5.66
74	N	Q	0.00	-4.29	5.91	0.00	-11.00	-3.44	-7.56	13.75	1.60	12.14	14.66	10.45	4.21	2.97	-3.06	6.03
75	S	N	-1.22	-4.66	-1.17	0.31	-7.17	7.22	-14.40	-35.76	-4.34	-31.41	11.00	1.23	9.78	24.41	0.73	23.69
75	S	Q	4.75	-1.11	4.44	0.31	26.31	29.85	-3.54	-28.87	-6.92	-21.96	21.53	24.46	-2.94	21.00	2.33	18.68
76	Q	N	-1.61	1.19	-1.50	0.00	-9.37	-2.33	-7.04	0.44	-0.59	1.02	2.28	5.24	-2.97	6.07	-1.82	7.89
78	F	N	-4.58	0.00	0.00	0.00	3.34	0.46	2.89	5.48	5.98	-0.50	-3.23	3.50	-6.73	6.58	1.98	4.60
78	F	Q	0.00	0.00	-3.07	0.00	-11.05	-4.91	-6.15	-8.99	4.79	-13.79	-6.42	6.54	-12.97	2.47	-2.04	4.51
103	N	Q	-1.14	0.00	5.15	-0.04	-13.39	-0.59	-12.80	-22.49	-8.02	-14.47	-6.56	0.38	-6.94	-6.77	-3.88	-2.88

PTPS Decreased Binding																		
PTPS Residue			Per-Res ΔHBond				CSA Cavity			CSD Cavity			CSE Cavity			HEP Cavity		
num	from	to	CSA	CSD	CSE	HEP	ΔCav	Δ(HB+VDW)	ΔCou	ΔCav	Δ(HB+VDW)	ΔCou	ΔCav	Δ(HB+VDW)	ΔCou	ΔCav	Δ(HB+VDW)	ΔCou
68	K	N	7.58	0.00	5.88	9.87	95.67	8.45	87.22	79.75	-5.99	85.73	119.99	-3.28	123.26	137.68	1.17	136.51
68	K	Q	7.60	0.00	0.43	9.87	103.11	7.80	95.31	77.89	-4.12	82.01	116.16	-0.89	117.05	160.96	3.13	157.83
69	K	N	8.27	0.00	-0.43	0.41	109.55	12.56	96.99	87.95	5.61	82.35	84.90	-3.08	87.97	123.59	-1.29	124.88
69	K	Q	8.27	0.00	5.12	0.41	97.91	5.28	92.63	75.40	4.98	70.41	90.73	-5.27	95.99	135.29	-6.80	142.10
71	K	N	4.58	4.29	1.68	5.71	78.37	4.92	73.44	84.49	-3.90	88.39	74.38	-1.00	75.38	172.64	-0.70	173.34
71	K	Q	6.15	-2.56	0.20	11.24	89.01	13.20	75.81	74.24	-11.41	85.65	72.17	-1.89	74.06	185.03	13.95	171.08
77	R	Q	6.96	6.37	6.84	14.14	100.48	5.10	95.38	128.38	3.40	124.98	107.04	-9.98	117.03	163.36	0.66	162.70
77	R	N	7.01	0.96	11.82	14.14	94.89	2.33	92.57	130.30	-1.43	131.72	108.53	-10.16	118.69	165.41	0.61	164.81
97	R	N	4.59	9.78	-0.96	12.05	100.76	0.66	100.09	123.99	1.22	122.76	121.08	11.91	109.17	189.16	-0.56	189.72
97	R	Q	4.59	9.78	-0.05	6.35	91.62	-0.55	92.18	116.85	2.75	114.09	114.11	1.33	112.78	188.49	0.66	187.84
100	R	N	12.01	18.70	3.81	15.24	98.76	2.89	95.88	150.09	5.51	144.58	139.31	0.52	138.79	219.62	-1.39	221.02
100	R	Q	12.01	23.01	0.71	15.53	91.91	2.23	89.69	132.35	2.97	129.37	112.37	3.65	108.72	221.74	1.56	220.19

Figure S38 – Single residue mutation data for RPTPs. Values show change in binding energy (kcal/mol) relative to wild-type structures. Values are shown both for the change in hydrogen bonding for the specific mutated residue as well as the overall change in the full cavity binding energy. The cavity binding energy is further separated into hydrogen bonding + van der Waals or Coulomb energy.

NGR1 - Increased Binding (Relative Energy)					
Set	CSA	CSD	CSE	HEP	Mutations
G1	-15.8	-14.0	2.7	-3.6	C395Q C405N
G2	10.6	-30.8	4.2	-38.0	S396N N399Q C405N
G3	-0.1	0.4	10.5	-1.1	C395Q S396N S403Q C405Q
G4	-20.9	-19.6	9.8	-27.1	S396Q C405N

NGR1 - Decreased Binding (Relative Energy)					
Set	CSA	CSD	CSE	HEP	Mutations
L1	481.3	607.0	649.0	850.0	R390N R391N R392Q R402N R406N
L2	471.5	627.0	597.9	813.1	R390Q R391Q R400N R402N R406N
L3	382.4	463.0	580.7	610.0	R391N R392Q R402Q R406Q
L4	473.2	629.9	642.9	834.1	R390N R392Q R400N R402Q R406N

NGR1 - Increased Binding (Percent Change)					
Set	CSA	CSD	CSE	HEP	Mutations
G1	2.2	1.4	-0.3	0.3	C395Q C405N
G2	-1.5	3.1	-0.5	3.4	S396N N399Q C405N
G3	0.0	0.0	-1.2	0.1	C395Q S396N S403Q C405Q
G4	2.9	2.0	-1.1	2.4	S396Q C405N

NGR1 - Decreased Binding (Percent Change)					
Set	CSA	CSD	CSE	HEP	Mutations
L1	-65.3	-62.0	-71.3	-75.8	R390N R391N R392Q R402N R406N
L2	-64.0	-64.1	-65.7	-72.5	R390Q R391Q R400N R402N R406N
L3	-51.9	-47.3	-63.8	-54.4	R391N R392Q R402Q R406Q
L4	-64.2	-64.3	-70.6	-74.4	R390N R392Q R400N R402Q R406N

Figure S39 – Predicted sets of mutations to either increase (left) or decrease (right) binding of ligands to NgR1. Note that none of the sets show improved binding for CS-E. Changes in binding energy are shown relative to the wild-type structures in both absolute change in binding energy (kcal/mol) and in terms of percent change.

NGR1 Increased Binding																		
NGR1 Residue			Per-Res ΔHBond				CSA Cavity			CSD Cavity			CSE Cavity			HEP Cavity		
num	from	to	CSA	CSD	CSE	HEP	ΔCav	Δ(HB+VDW)	ΔCou	ΔCav	Δ(HB+VDW)	ΔCou	ΔCav	Δ(HB+VDW)	ΔCou	ΔCav	Δ(HB+VDW)	ΔCou
395	C	Q	-5.33	0.00	-4.87	0.00	-7.24	2.09	-9.33	3.60	-1.74	5.34	8.95	0.38	8.57	6.30	-3.63	9.93
396	S	N	0.00	-1.73	-6.06	0.00	-3.19	3.57	-6.76	-15.44	-3.64	-11.80	9.88	3.95	5.93	10.94	-3.36	14.31
396	S	Q	0.00	4.38	-0.05	-4.85	-6.51	3.69	-10.21	-0.97	1.83	-2.81	15.97	5.70	10.27	-13.35	-5.15	-8.19
399	N	Q	4.67	-3.26	0.00	0.00	2.86	2.29	0.58	-7.57	-2.71	-4.86	2.18	-0.67	2.85	-47.06	-1.26	-45.80
403	S	Q	0.00	0.00	-5.22	0.00	4.39	4.40	0.00	-3.76	-2.31	-1.45	5.82	2.99	2.84	-1.31	-4.93	3.62
405	C	N	-6.52	-4.36	-0.79	-3.27	-8.64	5.99	-14.62	-24.39	-5.79	-18.61	-0.64	-0.16	-0.47	-0.03	-7.67	7.65
405	C	Q	0.00	-1.60	-6.10	0.00	-4.76	8.05	-12.81	-4.87	5.03	-9.90	-3.39	-0.36	-3.04	-0.92	-5.56	4.64

NGR1 Decreased Binding																		
NGR1 Residue			Per-Res ΔHBond				CSA Cavity			CSD Cavity			CSE Cavity			HEP Cavity		
num	from	to	CSA	CSD	CSE	HEP	ΔCav	Δ(HB+VDW)	ΔCou	ΔCav	Δ(HB+VDW)	ΔCou	ΔCav	Δ(HB+VDW)	ΔCou	ΔCav	Δ(HB+VDW)	ΔCou
390	R	Q	0.86	8.12	0.00	14.17	83.82	3.55	80.28	127.85	4.00	123.84	74.90	-2.34	77.24	216.92	-6.24	223.17
390	R	N	3.65	7.85	0.00	20.17	91.45	4.43	87.03	129.28	7.46	121.83	103.46	1.07	102.40	214.66	5.94	208.73
391	R	N	12.39	1.33	4.80	0.00	111.02	12.01	99.03	117.11	-3.64	120.74	133.74	3.22	130.51	104.52	-5.12	109.65
391	R	Q	12.39	5.69	4.80	0.00	81.87	1.91	79.96	108.81	6.44	102.37	130.43	2.71	127.72	116.57	-6.14	122.71
392	R	N	5.47	-0.86	10.62	6.61	87.18	6.33	80.86	120.25	11.02	109.24	165.18	11.93	153.25	176.91	4.80	172.12
392	R	Q	5.93	-0.64	10.64	7.72	88.87	5.06	83.81	111.70	3.80	107.91	165.48	10.73	154.75	175.74	3.43	172.31
400	R	N	0.88	15.38	0.00	5.59	75.35	3.35	72.00	140.99	10.79	130.20	95.87	-1.00	96.87	141.97	-4.20	146.17
400	R	Q	0.95	11.95	0.00	5.57	88.95	9.99	78.97	135.65	8.85	126.80	93.43	-0.12	93.56	108.39	-2.58	110.97
402	R	Q	7.41	5.08	12.90	4.13	78.45	8.42	70.03	107.96	-4.30	112.26	147.99	4.21	143.78	142.76	-4.02	146.78
402	R	N	7.47	6.67	0.70	2.92	84.77	9.26	75.52	110.69	-4.12	114.81	144.72	3.64	141.08	149.66	-3.21	152.87
406	R	Q	6.16	2.32	13.46	5.97	91.65	9.39	82.27	86.91	-5.04	91.95	136.94	2.12	134.82	167.79	2.68	165.11
406	R	N	7.34	4.44	12.49	5.97	103.23	11.66	91.57	97.02	3.78	93.24	135.69	1.72	133.98	181.99	-1.47	183.46

Figure S40 – Single residue mutation data for NgR1. Values show change in binding energy (kcal/mol) relative to wild-type structures. Values are shown both for the change in hydrogen bonding for the specific mutated residue as well as the overall change in the full cavity binding energy. The cavity binding energy is further separated into hydrogen bonding + van der Waals or Coulomb energy.

NGR3 - Increased Binding (Relative Energy)					
Set	CSA	CSD	CSE	HEP	Mutations
G1	-15.9	6.9	-9.9	-10.1	I345Q A348N
G2	-3.1	0.8	-10.2	-0.1	I345Q
G3	-12.9	-5.1	-5.8	-12.2	A348N
G4	-7.7	1.9	7.9	-23.7	N338Q A348N

NGR3 - Decreased Binding (Relative Energy)					
Set	CSA	CSD	CSE	HEP	Mutations
L1	230.6	271.2	327.7	396.5	K331N K334Q R342N
L2	321.9	537.6	545.0	802.2	K331N R342N R380N R381N R383N
L3	470.9	771.7	858.4	1054.7	R330N K331N K334N R342N R380Q K381N K383N
L4	238.0	413.9	425.4	644.0	R340N R379N R380N R383N

NGR3 - Increased Binding (Percent Change)					
Set	CSA	CSD	CSE	HEP	Mutations
G1	2.2	-0.6	0.8	0.7	I345Q A348N
G2	0.4	-0.1	0.8	0.0	I345Q
G3	1.8	0.4	0.5	0.8	A348N
G4	1.0	-0.2	-0.6	1.5	N338Q A348N

NGR3 - Decreased Binding (Percent Change)					
Set	CSA	CSD	CSE	HEP	Mutations
L1	-31.3	-23.6	-27.0	-25.9	K331N K334Q R342N
L2	-43.7	-46.8	-44.9	-52.4	K331N R342N R380N R381N R383N
L3	-63.9	-67.1	-70.7	-68.9	R330N K331N K334N R342N R380Q K381N K383N
L4	-32.3	-36.0	-35.0	-42.1	R340N R379N R380N R383N

Figure S41 – Predicted sets of mutations to either increase (left) or decrease (right) binding of ligands to NgR3. Changes in binding energy are shown relative to the wild-type structure in both absolute change (kcal/mol) and in terms of percent change.

NGR3 Increased Binding																		
NGR3 Residue			Per-Res ΔHBond				CSA Cavity			CSD Cavity			CSE Cavity			HEP Cavity		
num	from	to	CSA	CSD	CSE	HEP	ΔCav	Δ(HB+VDW)	ΔCou	ΔCav	Δ(HB+VDW)	ΔCou	ΔCav	Δ(HB+VDW)	ΔCou	ΔCav	Δ(HB+VDW)	ΔCou
338	N	Q	1.43	0.06	3.53	-5.31	-4.84	2.39	-7.23	6.70	0.74	5.96	18.28	-2.09	20.37	0.10	1.74	-1.64
345	I	Q	-4.24	-5.59	0.00	0.00	-3.12	-0.93	-2.20	0.80	-3.97	4.78	-10.18	-7.76	-2.41	-0.10	-0.19	0.08
348	A	N	-4.60	0.00	-0.78	-2.15	-12.91	-2.87	-10.04	-5.07	-2.65	-2.42	-5.76	-1.24	-4.51	-12.19	-3.71	-8.48

NGR3 Decreased Binding																		
NGR3 Residue			Per-Res ΔHBond				CSA Cavity			CSD Cavity			CSE Cavity			HEP Cavity		
num	from	to	CSA	CSD	CSE	HEP	ΔCav	Δ(HB+VDW)	ΔCou	ΔCav	Δ(HB+VDW)	ΔCou	ΔCav	Δ(HB+VDW)	ΔCou	ΔCav	Δ(HB+VDW)	ΔCou
330	R	N	0.74	-1.09	9.03	0.08	84.09	9.33	74.77	49.41	-4.51	53.92	149.89	2.24	147.65	125.52	-3.79	129.32
330	R	Q	0.74	-2.10	7.54	-0.17	84.81	10.32	74.49	28.03	-5.77	33.80	152.89	2.27	150.63	127.01	-5.33	132.33
331	K	Q	4.31	5.31	1.87	-2.08	92.34	0.99	91.35	25.97	-7.63	33.60	105.28	6.51	98.78	155.28	-2.14	157.42
331	K	N	7.53	5.75	1.87	-6.82	101.31	7.32	94.00	31.23	-5.72	36.95	100.70	6.15	94.55	148.88	-1.89	150.77
334	K	N	2.01	-6.09	9.00	0.00	70.93	-2.08	73.02	70.93	-6.27	77.20	154.48	-2.05	156.53	119.55	-2.40	121.96
334	K	Q	6.57	0.00	3.57	0.00	53.70	1.07	52.63	93.72	-3.94	97.67	102.98	-2.46	105.44	130.15	-0.69	130.84
340	R	N	0.00	-1.29	0.00	5.17	64.44	1.69	62.74	117.17	-4.79	121.96	73.59	-5.51	79.09	112.55	-10.32	122.87
340	R	Q	0.00	-1.28	0.00	5.17	64.45	0.34	64.11	72.83	-7.89	80.72	77.98	-11.87	89.85	120.72	-7.44	128.16
342	R	N	8.86	16.64	5.66	0.00	71.30	4.52	66.77	128.14	0.11	128.03	95.01	-5.88	100.89	108.88	-8.34	117.22
342	R	Q	8.86	16.07	5.66	0.00	63.84	3.86	59.98	126.70	-0.15	126.85	92.95	-4.70	97.65	108.36	-6.29	114.65
379	K	N	0.00	0.00	0.00	5.58	3.64	-4.34	7.99	76.86	-2.33	79.19	82.12	-1.28	83.39	158.63	2.23	156.40
379	K	Q	0.00	0.00	0.00	5.58	11.27	2.03	9.24	72.12	-1.96	74.08	84.91	-0.05	84.96	158.55	-1.94	160.48
380	R	N	0.00	5.43	0.59	3.93	42.61	-0.06	42.68	51.23	0.39	50.85	66.95	-3.91	70.86	188.74	-3.93	192.67
380	R	Q	0.00	5.43	2.81	1.21	35.33	0.26	35.08	45.62	-0.61	46.23	69.83	-10.08	79.91	196.39	-3.00	199.40
381	K	N	0.00	4.69	8.58	1.68	56.14	2.87	53.27	84.96	-2.92	87.89	119.97	-5.89	125.86	146.31	-14.85	161.17
381	K	Q	0.00	4.69	8.27	-7.65	47.50	0.85	46.65	110.48	-0.09	110.57	120.14	-4.00	124.14	137.24	-17.81	155.05
383	K	Q	-5.14	6.10	2.09	6.77	42.26	2.69	39.58	63.75	-7.34	71.09	95.05	-3.91	98.96	154.07	-9.80	163.87
383	K	N	0.00	6.10	10.92	7.95	42.16	1.41	40.75	60.25	-2.41	62.66	92.99	-2.73	95.71	176.79	-5.68	182.47

Figure S42 – Single residue mutation data for NgR3. Values show change in binding energy (kcal/mol) relative to wild-type structures. Values are shown both for the change in hydrogen bonding for the specific mutated residue as well as the overall change in the full cavity binding energy. The cavity binding energy is further separated into hydrogen bonding + van der Waals or Coulomb energy.